This is a peer-reviewed, accepted author manuscript of the following research article:
Bao, H., Shen, J., Liu, Y., & Chen, H. (2022). Shakedown analysis and assessment method of four-stress parameters Bree-type problems. International Journal of Mechanical Science, [107518]. https://doi.org/10.1016/j.ijmecsci.2022.107518

Shakedown analysis and assessment method of four-stress parameters Bree-type problems

Hongchen Bao[1], Jun Shen[2], Yinghua Liu[1*], Haofeng Chen[3, 4*]

1. Department of Engineering Mechanics, AML, Tsinghua University, Beijing, 100084, China
2. School of Energy and Power Engineering, University of Shanghai for Science and Technology, Shanghai, China
3. Key Laboratory of Pressure Systems and Safety (DOE), School of Mechanical and Power Engineering, East China University of Science and Technology, Shanghai, 200237, China
4. Department of Mechanical and Aerospace Engineering, University of Strathclyde, 75 Montrose Street, Glasgow G1 1XJ, Scotland, United Kingdom

Abstract：

For pressure equipment in the industrial field, the shakedown design methods presented in the ASME and other international design codes are mainly based on the Bree problem. The original Bree problem and its related modified Bree problems usually contain two types of stress parameters, whereas design by analysis based on the stress categorisation of the codes actually includes multiple types of stress parameters. In this paper, the four-stress parameters Bree-type shakedown problems (involving mechanical membrane and bending as well as thermal membrane and bending) have been studied under three typical thermo-mechanical loading conditions for the first time to reveal the mechanisms of the four-dimensional Bree diagram. A detailed discussion on the mechanical models for various uniaxial Bree-type problems is conducted to clarify the scope of application and mechanical assumptions for each problem. A common finite element model is developed for all discussed Bree-type problems. The Linear Matching Method (LMM) is utilised to construct the shakedown boundaries of three examples under three loading conditions, and the semi-analytical parametric equations of the shakedown boundaries are derived based on the numerical results and four-dimensional ratcheting boundary theory. Using the idea of a minimum shakedown boundary, a unified and conservative shakedown assessment scheme is proposed for the four-stress parameters Bree-type problems. The newly presented results can enhance the understanding of the structural behaviour of pressure equipment for many loading conditions and guide shakedown design and ratcheting assessment of practical industrial components.

Keywords： Shakedown analysis, Ratcheting assessment, Linear matching method, Bree-type problem, Cyclic loading

*Corresponding author email:[1] yhliu@tsinghua.edu.cn, [4] haofeng.chen@strath.ac.uk

1. **Introduction**

Shakedown is a beneficial concept in plastic mechanics, and it means that a certain amount of plastic deformation occurs after the initial several load cycles, resulting in a favourable time-independent residual stress field. The elastic limit load of the body is enhanced, and the structure behaves elastically in the subsequent load cycles after shakedown. Compared with pure elastic design, shakedown analysis takes advantage of the plastic behaviour of the material and excavates the load-bearing potential of the structure. Therefore, it can save materials, reduce resource consumption, and improve the economy while ensuring safety. For pressure-bearing equipment in the petrochemical, nuclear power, aerospace and other industrial fields, such as cracking furnaces, high-temperature boilers, and industrial pipelines, it is necessary to ensure that structures and components meet the shakedown condition to avoid plastic collapse caused by incremental plastic deformation (ratcheting) and low cycle fatigue associated with the alternating plasticity [1-23].

As for the shakedown design of pressure equipment such as vessels and piping, the analysis methods given in the leading international design codes (such as ASME VIII-2 [24], ASME III-NB [25], ASME III-NH [26], EN 13445-3 [27]) are based on the Bree problem. The thermal stress ratcheting assessment code rules were developed from the Bree ratcheting boundary equations for components subjected to medium- and low-temperature variation ranges. For the shakedown design of high-temperature components, the main idea of the simplified inelastic analysis method is to adopt the modified Bree diagram considering the effective creep stress parameter. Although Bree's work [28,29] laid the foundation for the shakedown design and ratcheting assessment of pressure equipment, many basic assumptions were adopted in the original Bree problem to simplify the analytical derivation. The Bree problem considers an axisymmetric cylindrical shell model; since the axial stress and radial stress are ignored, it can be regarded as a uniaxial ratcheting problem of a rectangular section beam, and only two types of stress parameters in the hoop direction of the shell are considered, i.e., mechanical membrane and thermal bending.

Over the past decades, many modified Bree problems and related modified Bree diagrams that broke the basic assumptions of the original Bree problem have been continuously developed. For instance, Bradford [30,31] and some other scholars [32-35] considered the influence of more types of thermo-mechanical loading conditions and established modified Bree diagrams applicable to in-phase and out-of-phase loading through cycle-by-cycle derivation. Pei et al.[36] recently have developed a universal procedure that can generate modified Bree diagrams with arbitrary phase shifts between the thermal and mechanical loads. Peng et al.[1] studied the shakedown regions of Bree problems considering three types of loading numerically based on the stress compensation method. O'Donnell and Porowski [37,38] developed the elastic core stress diagram based on the Bree problem, which can be used to evaluate creep ratcheting and creep fatigue of high-temperature components. Bradford[39] and McGreevy[40] developed modified Bree diagrams involving the effects of different yield strengths during the start-up and shutdown stages. Peng[41]derived modified Bree shakedown boundaries with the yield stress linearly dependent on temperature gradient using the non-cyclic method. Nayebi et al.[42,43] extended the Bree diagram by considering damage mechanics and strain hardening, and the effects of strain hardening on the Bree diagram have also been studied by Pei et al.[34,

44]. Since the original Bree problem is uniaxial, Bree and other scholars [45-49] have also developed some biaxial stress modified Bree diagrams; however, the biaxial stress Bree diagrams have not been widely used due to the over-conservatism. Hasbroucq et al.[9] derived the modified Bree diagram of thin plate considering the temperature dependence of Young's modulus and Poisson's ratio. Recently, the Bree diagram has been extended by Liu et al.[10]to involve progressive buckling failure, and it is shown by Ma et al.[2] that constant fatigue life curves can be incorporated into Bree-like diagrams for unified ratcheting and fatigue analysis. Although much progress has been accumulated over the past few decades on modified Bree problems and modified Bree diagrams, the shakedown analysis methods adopted by the mainstream codes and standards are still based on the classical uniaxial Bree problem due to its groundbreaking guidance and effectiveness in engineering. However, for the main international design codes of pressure equipment, design by analysis based on the stress categorisation actually includes some other types of stress parameters that were not considered by the original Bree problem, such as the thermal membrane and mechanical bending. Consequently, there is a mismatch between the original theory and practical engineering application of the Bree problem. It is important to study the multi-stress parameters modified Bree problems and corresponding multi-dimensional modified Bree diagrams further.

Due to the adoption of many basic assumptions, there are always some inherent conservative and non-conservative issues about the Bree problem. It is pointed out that the original Bree problem has limitations in situations involving high thermal membrane stress [50,51]. To solve the inherent non-conservatism of the Bree problem, Reinhardt [50] derived a three-dimensional (3D) ratcheting boundary based on the rectangular beam model using the non-cyclic method [52-54]. The influence of the thermal membrane was added so that the Bree ratcheting boundary became a sideline of the ratcheting boundary established by Reinhardt. Since the 2013 edition of ASME VIII-2 [55], the ratcheting check on thermal membrane stress has been supplemented; however, the primary bending stress is not involved in the thermal stress ratcheting assessment. In 2018, Shen et al. [56] considered the influence of primary bending stress in shakedown analysis and established a four-dimensional (4D) ratcheting boundary, which involves the four most common thermo-mechanical stress parameters of the stress categorisation method. The four-stress parameters ratcheting theory is of considerable value since there are relatively few closed-form theoretical solutions to ratcheting problems. However, the four-dimensional ratcheting boundary formulas are too complicated and must be further simplified and analysed to be suitable for engineering applications.

For the original 2D Bree diagram, 3D Reinhardt's ratcheting boundary and 4D Shen's ratcheting boundary mentioned above, the loading conditions are of the same type, i.e., constant primary load and cyclic thermal load. Much progress has been made in extending the 2D Bree diagram to generalised loading conditions over the past few decades [30-36], but to the authors' knowledge, similar extensions to 3D and 4D shakedown and ratcheting boundaries are rare due to the difficulty of the cycle-by-cycle derivation. In fact, the 3D and 4D ratcheting boundaries are derived by the non-cyclic method [52-54], which is confined to the classical Bree-type loading. Recently, the 3D Reinhardt-type shakedown boundary has been studied under different loading conditions [57], however, the shakedown behaviour of the four-stress parameters Bree-type

problem under complex loading conditions is still unknown, which constitutes the research goal of this paper. Compared with the two-stress parameters and three-stress parameters shakedown problems, the four-stress parameters shakedown problems are more complex. The complexity comes from three aspects. One aspect is the difficulty of mathematics, the 4D ratcheting boundary is controlled by seven complicated equations, and the four-stress parameters problem can actually plot an infinite number of 3D shakedown and ratcheting boundaries, so it is difficult to grasp the essential characteristics of the shakedown and ratcheting boundaries. Another aspect of complexity lies in the relationships among four-stress parameters problems and two-stress parameters and three-stress parameters problems, especially after introducing complex loading conditions. For example, whether the four-stress parameters problem can degenerate into the two-stress parameters and three-stress parameters problems. The third aspect of complexity is how to conservatively represent the 4D shakedown boundary for shakedown assessment in engineering applications.

For generalised loading conditions, the analytical cycle-by-cycle derivation of the multi-stress parameters Bree-type problem is cumbersome and laborious, and experimental research is usually impractical due to the high cost and complex influencing factors. Extensive work has shown that numerical simulation is a desirable research method for shakedown problems, especially the direct methods with both efficiency and accuracy based on the classical upper bound [58] and lower bound [59] shakedown theorems. The upper bound shakedown theorem, also known as the kinematic shakedown theorem of Koiter, seeks the upper bound shakedown limit based on the minimization of plastic dissipation energy; While the lower bound shakedown theorem, also known as the static shakedown theorem of Melan, seeks the lower bound shakedown limit by ensuring the superposition of constant residual stress field and fictitious elastic stress field satisfy the yield condition everywhere. Shakedown analysis based on the shakedown theorems can usually be transformed into solving mathematical programming problems. Over the past few decades, some optimization approaches have been proposed for solving the mathematical programming problem, such as the second order cone programming (SQCP)[60] and the interior point method (IPM)[61]. However, optimization algorithms usually encounter mathematical difficulties and computational scale problems when dealing with complex engineering problems. Going around the mathematical difficulties of optimization approaches, some direct methods of shakedown analysis based on the mechanical perspective have been developed, such as the linear matching method (LMM)based on upper bound shakedown theorem and stress compensation method (SCM) based on lower bound shakedown theorem. The key point of LMM is to construct the kinematically admissible strain rate and to approximate nonlinear plastic behaviour with linear solutions by adjusting the modulus. While the key point of SCM is to search for the statically admissible residual stress field and satisfy the yield condition by applying compensation stress. It is shown in references [1,4] that the computational efficiency of the SCM and LMM for complex engineering problems is basically one order of magnitude higher than that of finite element step-by-step analysis. Among the many direct methods that have been developed, the LMM is relatively robust and mature, and both the upper bound and lower bound procedures have been established. Many examples have shown that the LMM can effectively solve a series of structural integrity problems, such as high temperature life integrity[62, 63], plastic behaviour and creep rupture

assessment[64-66], creep fatigue interaction[67,68], limit analysis of composite laminates[69-71], etc, and it has been introduced into the British R5 procedures [72].

This paper aims to reveal the mechanisms of the four-stress parameters Bree-type shakedown problems under three thermal-mechanical loading conditions based on the upper bound Linear Matching Method (LMM) and four-dimensional ratcheting boundary theory, and to propose the corresponding shakedown assessment methods under different loading conditions. The logical structure of this paper is as follows. The mechanical models for various uniaxial Bree-type problems are discussed in Section 2, and a common finite element model for all discussed Bree-type problems is developed in Section 3. Some typical cases of the four-stress parameters Bree-type shakedown problems are systematically studied in Section 4 under three loading conditions. A unified and conservative shakedown assessment scheme is proposed for the four-stress parameters Bree-type problems in Section 5. Conclusions are given in Section 6.

2. **Discussion on the mechanical models for various uniaxial Bree-type problems**

In this section, four kinds of uniaxial Bree-type problems with different stress parameters are discussed systematically to clarify the respective mechanical models and scope of application. The Bree-type problems considered in this section refer to the theories constructed by derivation or extended by numerical procedures based on the uniaxial rectangular beam model. The two-stress parameters Bree-type problems refer to the work presented by Bree[28-29], Bradford[30-31], Pei[36,44], etc. Examples of the three-stress parameters Bree-type problems are Reinhardt[50], Adibi-Asl[68], Bao[57], etc. The four-stress parameters Bree-type problem refers to the work of Shen[56]. Note that all considered three-stress and four-stress parameters problems can degenerate into the classical Bree problem.

2.1 Mechanical models of Bree-type problems applicable to thin-walled cylinders

The problems discussed in this subsection include the classical two-stress parameters Bree-type problems and the three-stress parameters Bree-type problem (named Type-A)[50, 57].

The two-stress parameters Bree-type problem was initially analysed for the strain behaviour of the reactor fuel clad made of elastic-perfectly plastic material. Therefore, the mechanical model is a thin-walled axisymmetric cylindrical shell with closed ends ((a)-(b) of Fig.1). The effects of end and curvature can be ignored by assuming $l ? D ? 2t$, where l is the length of the vessel, D is the diameter, and t is the thickness of the wall. In order to simplify the theoretical analysis and derive a closed-form analytical solution, only the combined thermal and mechanical stresses in the circumferential direction were considered. The hoop stresses can be applied on a rectangular section beam, and the stress distributions are shown by (c) of Fig.1, where subscript b means bending, m means membrane, p denotes primary and s denotes secondary. The bending stress is caused by radial cyclic linear temperature gradient ΔT_r, and the membrane stress is caused

by constant internal pressure P. It is assumed that the combined stresses do not cause the rotation of the beam to reflect the actual condition of the shell.

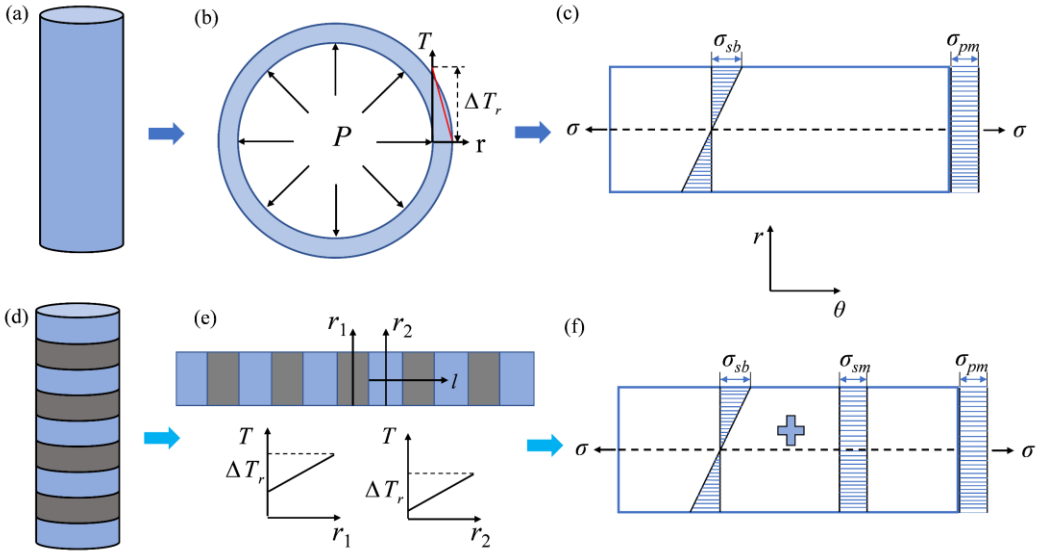

Fig.1. Mechanical models of the two-stress parameters((a)-(c)) and the Type-A three-stress parameters ((d)-(f)) Bree-type problems. (a) thin-walled cylindrical shell. (b) the sectional view of the shell with internal pressure P and uniform through-wall temperature gradient $\triangle T_r$. (c) stress distributions on a rectangular section beam corresponding to hoop direction (θ) of the shell with radial (r) temperature gradients. (d) cylindrical shell with uniform axial (l) temperature gradients. (e) through-wall temperature gradients along the axial direction of the shell. (f) stress distributions on a rectangular section beam corresponding to the hoop direction of the shell with axial temperature gradients.

The Type-A three-stress parameters Bree-type problem (σ_{sb}, σ_{sm}, σ_{pm}) considered in this section also applies to the cylindrical shell structure, but with additional axial temperature gradients. The thermal stress caused by the combined radial and axial temperature gradients can be divided into membrane stress and bending stress. The corresponding mechanical model and stress distributions of the Type-A three-stress parameters Bree-type problem are shown in (d)-(f) of Fig.1, where Fig. 1d represents a cylindrical shell with continuous axial temperature gradients and Fig. 1e displays the through-wall temperature gradients along the axial direction of the shell. The linear through-wall temperature gradient $\triangle T_r$ in the radial direction is assumed to be uniform, but the average temperatures of adjacent colour blocks in the axial direction are different, representing the axial thermal discontinuities. It is assumed that the thermal discontinuities are sufficiently continuous, and the stress fields are uniformly distributed. Obviously, when $\sigma_{sm}=0$, the Type-A three-stress parameters Bree-type problem can be reduced to the two-stress parameters Bree-type problem.

2.2 Mechanical models of Bree-type problems applicable to straight pipes

The problems discussed in this subsection include the three-stress parameters Bree-type problem (named Type-B) [73] and the four-stress parameters Bree-type problem[56].

The Type-B three-stress parameters Bree-type problem (σ_{sb}, σ_{pm}, σ_{pb}) adds the effect of primary bending stress σ_{pb} compared to the original two-stress parameters Bree-type problem. When $\sigma_{pb} \neq 0$, the application scope of this problem has changed compared with subsection 2.1, as shown in Fig.2. The rectangular section beam problem in Fig. 2 can be used as an approximation to the ratchet problem of straight pipe [74,75]. This problem will be more intuitive if the rectangular section is replaced with a thin-walled pipe cross-section, as shown by Fig. 2(a). The axial mechanical stresses can be caused by constant pressure, dead weight or other external loads. The thermal stress can be caused by cyclic temperature gradients between the upper and lower surfaces of the pipe. The through-wall temperature gradient is not under consideration, which is different from the classical Bree problem.

For the four-stress parameters Bree-type problem, the thermal stress is caused by the combined axial and surface temperature gradients, as shown by (b) and (d) of Fig. 2. The four-stress parameters Bree-type problem can degenerate into six kinds of two-stress parameters shakedown problems in total, including the original and inverse Bree problems. Besides, four kinds of three-stress parameters shakedown problems can be obtained from the four-stress parameters Bree-type problem, i.e., the case with $\sigma_{pb} = 0$ (named Type-a), the case with $\sigma_{sm} = 0$ (named Type-b), the case with $\sigma_{pm} = 0$ (named Type-c), the case with $\sigma_{sb} = 0$ (named Type-d). Since the Type-c and Type-d cases cannot degenerate into the classical Bree problem, they will not be discussed here. When $\sigma_{sm} = 0$, the results in Section 4.2 show that the Type-b case is identical to the Type-B three-stress parameters Bree-type problem. However, despite being very similar, the comparisons in Section 4.1 show that the Type-a case is different from the Type-A three-stress parameters Bree-type problem. This imperceptible and confusing difference deserves attention.

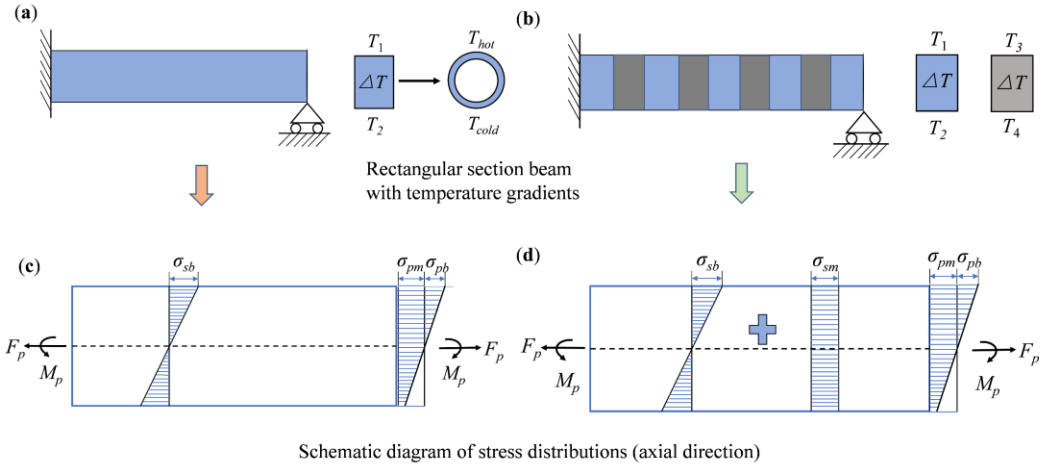

Fig.2. Mechanical models of the Type-B three-stress parameters ((a) and (c)) and four-stress parameters ((b) and (d)) Bree-type problems. (a) a rectangular section beam with uniform surface temperature gradients between the top and bottom. (b) a rectangular section beam with uniform surface and axial temperature gradients. (c) stress distribution characteristics of the Type-B three-stress parameters Bree-type problem. (d) stress distribution characteristics of the four-stress parameters Bree-type problem, where the thermal stress (σ_{sb} plus σ_{sm}) has five typical distribution patterns[50,56].

3. A common finite element model for uniaxial Bree-type problems

At present, several finite element models have been proposed to simulate the classical two-stress parameters Bree problem, such as the plane stress model[1, 76], axisymmetric model[77], two-bar model and N-bar model[78,79]. An axisymmetric axial thermal gradient FE model is adopted to illustrate the non-conservatism of the two-stress parameters Bree problem and simulate the thermal membrane stress of the Type-A three-stress parameters Bree-type problem [50]. A two-plane model was proposed for the numerical verification of the four-stress parameters Bree-type ratcheting problem through cycle-by-cycle FEA [56]. In order to simplify the numerical simulation and facilitate the comparison of various problems, a common FE model will be developed for all the uniaxial Bree-type problems considered in Section 2 based on the modified two-plane model. The FE model implementation methods corresponding to each problem will be compared to facilitate the understanding of the differences among various problems.

A modified two-plane model can be used for all the uniaxial Bree-type problems considered in Section 2, as shown in Fig.3. The element type is CPS8 in ABAQUS. The two planes are rigidly coupled in the direction-2 by the red reference point. For the two-stress parameters and Type-A three-stress parameters Bree-type problems, the rotational degree of freedom of the reference point needs to be fully suppressed, which is different from the Type-B three-stress parameters and four-stress parameters Bree-type problems. It is assumed that the cyclic temperature gradients of both planes in the direction-1 are linear. The thermal bending stress is controlled by the temperature gradient $2T$ in the direction-1 and $\sigma_{sb} = E\alpha T$. The thermal membrane stress is governed by the mean temperatures T_{m1} and T_{m2} of both planes. For the two-stress parameters and Type-B three-stress parameters Bree-type problems, $T_{m1} + T_{m2} = 0$. For the Type-A three-stress parameters and four-stress parameters Bree-type problems, $T_{m1} + T_{m2} \neq 0$. The mechanical stresses F and M can be applied directly to the reference coupling point. By changing the combinations of the four types of stresses, rotation conditions and applied temperature fields, the modified two-plane model can apply to all uniaxial Bree-type problems considered in Section 2.

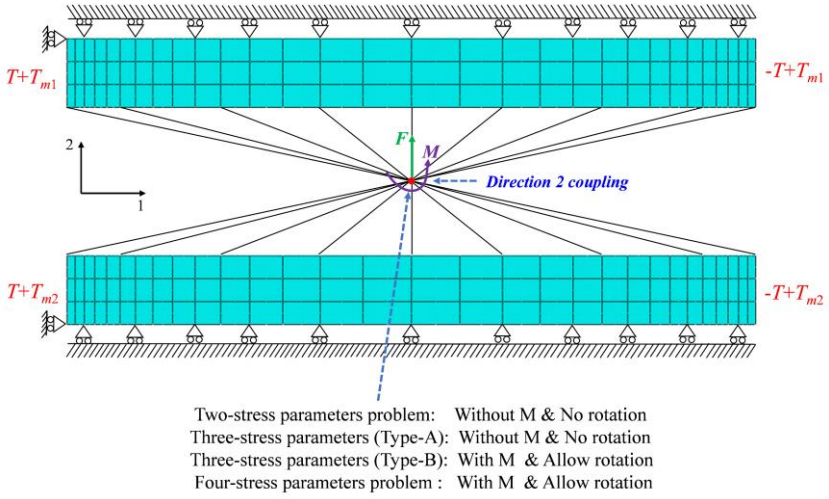

Fig.3. A common FE model for the Bree-type problems considered in Section 2.

4. Shakedown Analysis of the four-stress parameters Bree-type problems

In this section, three examples of the four-stress parameters Bree-type shakedown problems are investigated by numerical analysis and semi-analytical derivation under three typical loading conditions, as shown in Fig.4. Loading case I is the classical Bree-type loading, where the thermal stress σ_t and mechanical stress σ_p vary in the ranges of $0 \le \sigma_t \le \lambda_T \sigma_{t0}$ and $\sigma_p = \lambda_p \sigma_{p0}$. λ_T and λ_p are two multipliers for thermal and mechanical loads; σ_{t0} and σ_{p0} are two preset elastic stresses. For loading case II, σ_t and σ_p vary proportionally, i.e., in-phase loading, where $0 \le \sigma_t \le \lambda_T \sigma_{t0}$ and $\sigma_p = \mu \sigma_t$. For loading case III, σ_t and σ_p vary independently, where $0 \le \sigma_t \le \lambda_T \sigma_{t0}$ and $0 \le \sigma_p \le \lambda_p \sigma_{p0}$, and the loading paths can be arbitrary within the domain ABCD. The upper bound LMM is adopted for strict shakedown analysis, and the numerical procedure (refer to Appendix A) has been implemented into ABAQUS using user subroutines. Following the assumption of the classical Bree problem, an isotropic ideal elastic-plastic material is adopted, and the analysis is confined to associative plasticity by assuming associated flow rule. Table 1 lists the basic temperature-independent material properties. It is worth mentioning that although specific material parameters are used here, the analysis results in the following are expressed in a dimensionless form, so they can be applied to other ideal elastic-plastic materials.

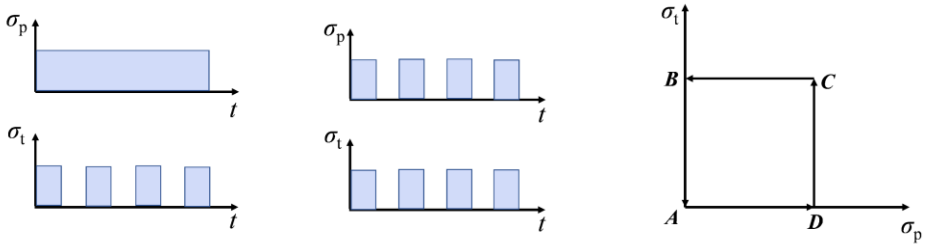

(a): loading case I: Bree-type (b) loading case II: in-phase (c) loading case III: vary independently

Fig. 4. Loading cases for shakedown analysis. For loading case I, σ_p remains constant, and σ_t keeps cycling. For loading case II, both σ_p and σ_t cycle continuously and vary proportionally. For loading case III, σ_p and σ_t can vary independently within their respective ranges.

Table 1. Material properties

Young 's modulus E (MPa)	2×10^5
Coefficient of thermal expansion α (/°C)	1×10^{-5}
Yield strength σ_y (MPa)	300
Poisson 's ratio v	0.3

In order to represent the four-dimensional shakedown boundary in a two-dimensional or three-dimensional coordinate system, it is necessary to specify at least one stress variable value or stress ratio value in advance. Several typical cases ($(\Delta)\sigma_{pb} = 0$, $\Delta\sigma_{sm} = 0$, $\Delta\sigma_{sb} = 0$, Δ means range) are selected in the

following to perform the shakedown analysis, study the variation of the shakedown boundaries, and establish the semi-analytical parametric equations correspondingly. It is shown that the three cases are sufficient to reveal the general variation trend of the four-dimensional shakedown boundary and clarify the differences among various Bree-type problems.

To quantitatively distinguish the influence of different types of stress parameters and facilitate the dimensionality reduction representation, the concepts of "primary membrane bending ratio" R_1 and "secondary thermal membrane bending ratio" R_2 are introduced in this paper, which are defined as follows:

$$R_1 = \frac{(\Delta)\sigma_{pm}}{(\Delta)\sigma_{pb}}, R_2 = \frac{\Delta\sigma_{sm}}{\Delta\sigma_{sb}} \tag{1}$$

4.1 Mechanical bending stress reduced to zero

For the original four-stress parameters ratcheting theory, when the thermal stress variation range $\Delta\sigma_t$ is less than twice the yield strength, that is, $\Delta\sigma_t \le 2\sigma_y$, the ratcheting boundary governing equations are as follows [56]:

a. When $\Delta\sigma_{sm} + \Delta\sigma_{sb} \le 2\sigma_y$ and $\Delta\sigma_{sm} \ge \Delta\sigma_{sb}$,

$$\sigma_{pb} = \frac{(3b^2 - 3a^2)\sigma_{pm} - \sqrt{2}(a^2 + b^2 - 2a\sigma_{pm} + 2b\sigma_{pm})^{\frac{3}{2}} + 2(a^3 + b^3)}{(a-b)^2} \tag{2}$$

where：

$$a = \sigma_y - \frac{\Delta\sigma_{sm} + \Delta\sigma_{sb}}{2} \tag{3}$$

$$b = \sigma_y - \frac{\Delta\sigma_{sm} - \Delta\sigma_{sb}}{2} \tag{4}$$

b. When $\Delta\sigma_{sm} + \Delta\sigma_{sb} \le 2\sigma_y$ and $\Delta\sigma_{sm} \le \Delta\sigma_{sb}$,

For $\sigma_{pm} \le \frac{(2\sigma_y - \Delta\sigma_{sb})\Delta\sigma_{sm}}{2\Delta\sigma_{sb}}$:

$$\sigma_{pb} = -\frac{1}{2\Delta\sigma_{sb}^2}\left(\begin{bmatrix} 2\sqrt{2}\left(\Delta\sigma_{sm} + 2\sigma_{pm}\right)\Delta\sigma_{sb} \\ +2\sigma_y(\sigma_y - \Delta\sigma_{sm}) \end{bmatrix}^{\frac{3}{2}} + \Delta\sigma_{sb}^3 - 3\Delta\sigma_{sb}^2\sigma_y + 12\Delta\sigma_{sm}\sigma_y^2 \right.$$
$$\left. -6(\Delta\sigma_{sm} + 2\sigma_{pm})(\sigma_y - \frac{1}{2}\Delta\sigma_{sm})\Delta\sigma_{sb} - 3\Delta\sigma_{sm}^2\sigma_y - 8\sigma_y^3 \right) \tag{5}$$

For $\sigma_{pm} > \frac{(2\sigma_y - \Delta\sigma_{sb})\Delta\sigma_{sm}}{2\Delta\sigma_{sb}}$:

$$\sigma_{pb}=-\frac{1}{2\Delta\sigma_{sb}^2}\left(\begin{array}{l}\left[\begin{array}{l}2\sqrt{2}\left(-\Delta\sigma_{sm}-2\sigma_{pm}\right)\Delta\sigma_{sb}\\+2\sigma_y(\sigma_y+\Delta\sigma_{sm})\end{array}\right]^{\frac{3}{2}}+\Delta\sigma_{sb}^3-3\Delta\sigma_{sb}^2\sigma_y-12\Delta\sigma_{sm}\sigma_y^2\\+6(\Delta\sigma_{sm}+2\sigma_{pm})(\sigma_y+\frac{1}{2}\Delta\sigma_{sm})\Delta\sigma_{sb}-3\Delta\sigma_{sm}^2\sigma_y-8\sigma_y^3\end{array}\right) \tag{6}$$

In the above formulas, $\Delta\sigma_{sm}$ denotes the variation range of thermal membrane stress, $\Delta\sigma_{sb}$ denotes the variation range of thermal bending stress, σ_{pm} denotes the constant mechanical membrane stress and σ_{pb} denotes the constant mechanical bending stress. Define the following variables: $\Delta\sigma_t=\Delta\sigma_{sm}+\Delta\sigma_{sb}$, $\sigma_p=\sigma_{pm}+\sigma_{pb}$, $X_{pm}=\sigma_{pm}/\sigma_y$, $X_{pb}=\sigma_{pb}/\sigma_y$, $Y=\Delta\sigma_{sb}/\sigma_y$, $Z=\Delta\sigma_{sm}/\sigma_y$, $X_p=\sigma_p/\sigma_y$, $Y'=\Delta\sigma_t/\sigma_y$.

In order to directly compare the Type-A and Type-a three-stress parameters Bree-type problems considered in Section 2, the mechanical bending stress in the four-stress parameters shakedown problem is reduced to zero. Assume $\sigma_{pb}=0$, then $1/R_1=0$. A series of R_2 values were assumed to perform the strict shakedown analysis. The convergence level is set as 1e-4 between successive asymptotic solutions to obtain the approximate limit multipliers. The variation range of thermal stress is:

$$\Delta\sigma_t=\sigma_t-0=\lambda^S\lambda_T\sigma_{t0} \tag{7}$$

where σ_{t0} denotes the preset maximum elastic thermal stress, λ^S and λ_T are the shakedown limit multiplier and thermal load multiplier, respectively.

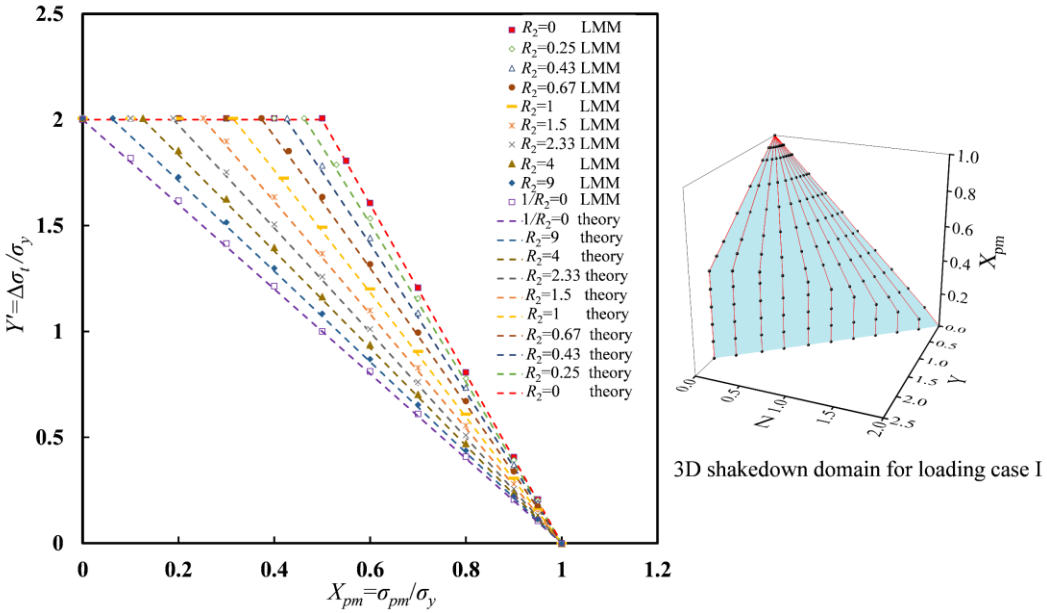

Fig. 5. Comparisons between the numerical results and theoretical solutions (Eqs. (2)-(6)) for the four-stress parameters Bree-type problem (σ_{pb}=0) under loading case I. Y'= Y+Z in this example denotes the dimensionless thermal stress range. The three-dimensional elastic shakedown domain is displayed in the $X_{pm}YZ$ coordinate system.

The calculation results for loading case I and the corresponding theoretical values (Eqs. (2)-(6)) are compared in Fig. 5. The results in Fig.5 show that the shakedown boundaries are composed of two segments except for the case of $1/R_2=0$. With the gradual increase of R_2, the shakedown regions decrease gradually. For different values of R_2, the shakedown regions always pass through two fixed points ($(X_{pm},Y')=(1,0)$ and $(X_{pm},Y')=(0,2)$) on the coordinate axes; the horizontal alternating plasticity boundary always remains unchanged, and the lower shakedown boundaries agree well with the four-stress parameters ratcheting boundaries. The corresponding three-dimensional shakedown domain in the $X_{pm}YZ$ coordinate system is also displayed in Fig.5.

Typical R_2 values were selected in Fig. 6 to compare the calculation results under different loading conditions. For different R_2 values, the boundaries are always the same under loading case II. The shakedown boundary for a given R_2 value under loading case III consists of two sections, in which the upper section overlaps with the shakedown boundary of loading case II, and the lower section overlaps with the shakedown boundary of loading case I. This conclusion is always valid in the analysis of this paper and is consistent with the conclusions obtained in the literatures [1,57] for the two-stress and Type-A three-stress parameters modified Bree problems. Fig. 6 also shows the corresponding three-dimensional elastic shakedown domains of loading case II and loading case III in the $\Delta X_{pm}YZ$ coordinate system, where $\Delta X_{pm}=\Delta\sigma_{pm}/\sigma_y$.

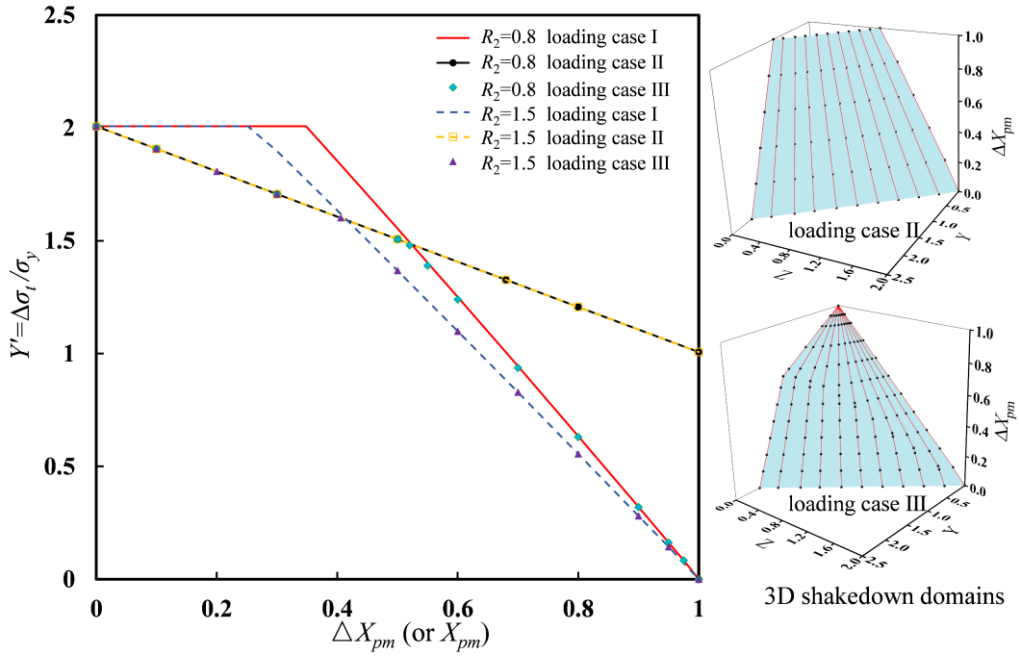

Fig. 6. Comparisons of the shakedown regions under different loading conditions for the four-stress parameters Bree-type problem when σ_{pb}=0. For loading case I, the coordinate system is $X_{pm}Y'$. For loading cases II and III, the coordinate system is $\triangle X_{pm}Y'$. Y'= Y+Z in this example denotes the dimensionless thermal stress range. The three-dimensional elastic shakedown domains under loading cases II and III are displayed in the $\triangle X_{pm}YZ$ coordinate system.

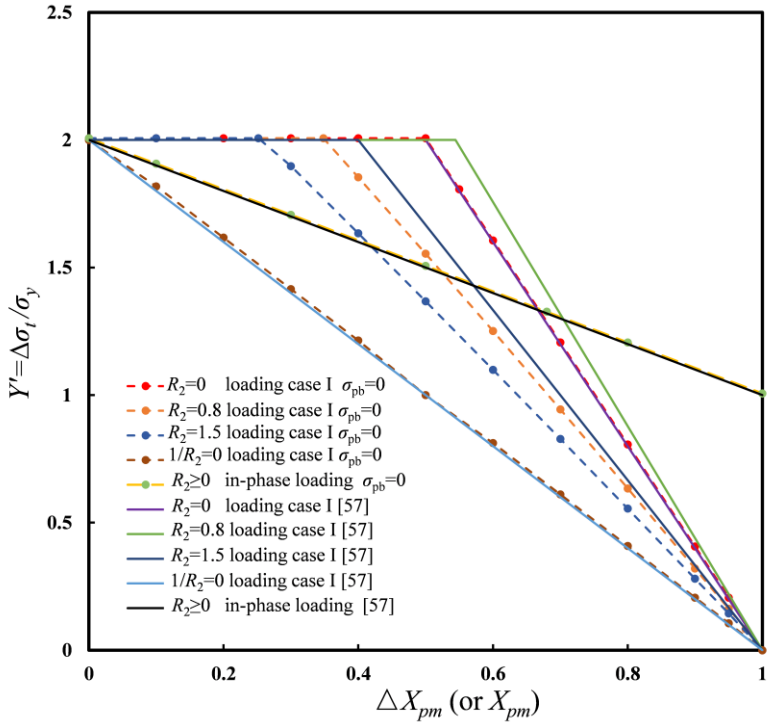

Fig. 7. Comparisons of the shakedown boundaries between the four-stress parameters Bree-type problem (σ_{pb}=0) and the Type-A three-stress parameters Bree-type problem under different loading conditions. For loading case I, the coordinate system is $X_{pm}Y'$. For loading case II, the coordinate system is $\Delta X_{pm}Y'$. The dashed lines with dots represent the calculation results of this section, and the solid lines are obtained from the parametric equations of the shakedown boundaries for Type-A three-stress parameters Bree-type problem studied in the literature [57].

Fig. 7 compares the calculation results in this section (Type-a three-stress parameters Bree-type problem) with the Type-A three-stress parameters Bree-type shakedown boundaries given by literature [57]. For the loading case I, when R_2=0 or $1/R_2$=0, the calculation results in this section are consistent with the literature [57]. However, when R_2 takes any other value, the calculation results in this section are more conservative, such as the comparison between the orange dashed line ($R_2=0.8$, Type-a) and the green solid line ($R_2=0.8$, Type-A) in Fig.7. This is because the stress action section of the Type-a problem can rotate compared with the Type-A problem. For most thermal stress distributions ($R_2\neq 0$ and $1/R_2\neq 0$), when the non-cyclic method is used for derivation, the residual yield stress distributions for final limit analysis are not symmetrical about the neutral axis of the beam. However, the primary membrane stress is symmetrical about the neutral axis, so primary bending stress is required to meet the equilibrium condition. Actually, except for the cases of R_2=0 and $1/R_2$=0, when the σ_{pm} reaches the maximum under any given thermal stress, the σ_{pb} calculated by substituting the Type-A three-stress parameters Bree-type problem into the four-stress parameters ratcheting theory is a negative value. Due to structural deformation constraints of the shell, the cross-section rotation of the beam is restricted for the Type-A problem, which implies a favourable and

negative primary bending stress, thereby improving the structural load-bearing capacity and expanding the shakedown region. Therefore, when $\sigma_{pb}=0$, the four-stress parameters ratcheting theory could not degenerate into the Type-A three-stress parameters Bree-type problem given by Reinhardt [50].

For loading case II, the shakedown limits are the same for the Type-A and Type-a three-stress parameters Bree-type problems, and are only controlled by the 3S criterion line. For loading case III, it can be concluded that the Type-a problem is still more conservative than the Type-A three-stress parameters Bree-type problem except for cases of R_2=0 and $1/R_2$=0.

4.2 Pure thermal bending stress case (R_2=0)

When $\Delta\sigma_{sm}=0$, the ratcheting boundary expression under loading case I can degenerate from Eq. (6) as follows:

For $\Delta\sigma_{sb}\le 2\sigma_y$:

$$\sigma_{pb}=\frac{[-8(-\sigma_{pm}\Delta\sigma_{sb}+\sigma_y^2)^{\frac{3}{2}}-12\sigma_y\Delta\sigma_{sb}\sigma_{pm}+3\Delta\sigma_{sb}^2\sigma_y+8\sigma_y^3-\Delta\sigma_{sb}^3]}{2\Delta\sigma_{sb}^2} \tag{8}$$

It is verified that Eq. (8) is equivalent to the ratcheting boundary formula given in the literature [73] for the rectangular section beam, although the formula forms look different. Therefore, when $\Delta\sigma_{sm}=0$, the four-stress parameters ratcheting theory could degenerate into the Type-B three-stress parameters Bree-type problem. As pointed out in the literatures [74,75], the problem considered in this section can be approximately applicable to straight pipes that ratchet in a beam mode. For the straight pipe problem, the primary stresses are actually the axial stresses, and the temperature gradient on the pipe wall thickness is not considered. However, for the thermal stress ratcheting problem considered by Bree [28] and Reinhardt [50], the primary stress corresponds to the hoop stress of the shell, and a linear temperature gradient is assumed through the wall thickness. As for the thin-walled pipe cross-section, the exact shakedown boundary expression is difficult to obtain explicitly, so the theoretical solutions based on the rectangular beam are of importance. In order to extend the application scope of the theoretical formulas, the shakedown boundary parametric equations under different loading conditions are established below.

Fig. 8 shows the calculation results of shakedown limits under loading case I, where X_p represents the dimensionless total primary stress, and the ordinate represents the dimensionless thermal bending stress. It is shown that the calculation results agree well with the theoretical values (Eq. (8)). With the gradual increase of R_1, the shakedown regions will first increase and then decrease. When the primary stress is pure mechanical membrane stress ($1/R_1$=0), the shakedown region will reach the minimum (the black dotted line in Fig. 8), which is equivalent to the Bree shakedown boundary. As the shakedown boundary can be conservatively regarded as composed of two straight lines, the general approximate form can be summarised, as shown in the lower-left corner of Fig. 8.

The parametric equations of the shakedown boundaries can be quickly constructed by determining the inflexion point coordinates X_p^c and plastic limit load coordinates X_p^f of the shakedown regions, where $X_p^f=X_{pm}^f+X_{pb}^f$. The relationship between X_{pm}^f and X_{pb}^f can be obtained from the plastic limit analysis of the rectangular beam, as shown by Eq. (9).

$$X_{pb}^f=\frac{3}{2}\left[1-\left(X_{pm}^f\right)^2\right] \tag{9}$$

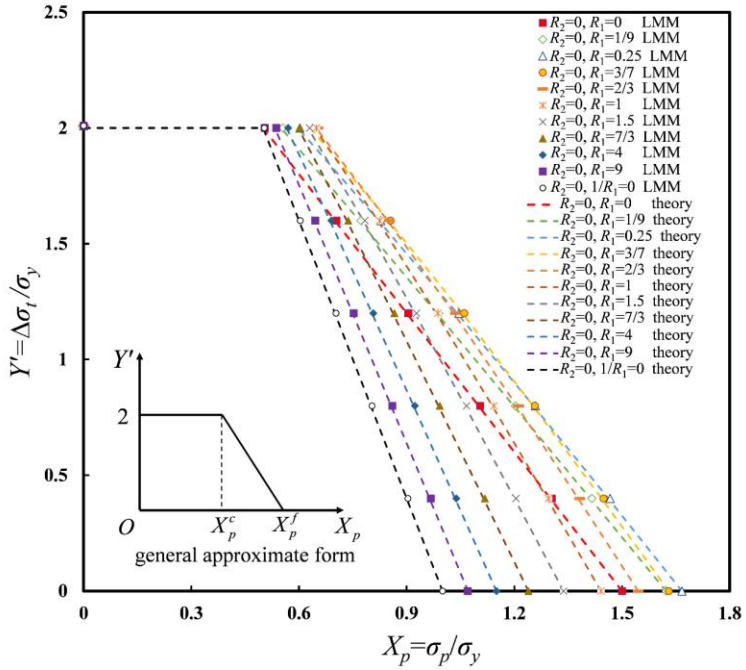

Fig. 8. Comparisons of the shakedown limit calculated results and theoretical solutions (Eq. (8)) under loading case I when R_2=0, where $\sigma_p=\sigma_{pm}+\sigma_{pb}$ and $Y'=Y$ in this example. The calculated results are shown by scatter points of various shapes, and theoretical solutions are presented by dotted lines. The results with R_2=0 & 1/ R_1=0 correspond to the shakedown boundary of the classical Bree problem.

When $\Delta\sigma_{sb}\to 0$, Eq. (9) can also be obtained from Eq. (8). Combined with $X_{pm}^f=R_1X_{pb}^f$, the expression of X_p^f can be derived as follows:

$$X_p^f=\frac{(1+R_1)(\sqrt{9R_1^2+1}-1)}{3R_1^2} \tag{10}$$

$X_p^f\to 1.5$ when $R_1\to 0$, and $X_p^f\to 1$ when $R_1\to+\infty$. Given $\Delta\sigma_{sb}=2\sigma_y$, it can be obtained from Eq. (8) that:

$$X_{pb}^c=\frac{3}{2}-(1-2X_{pm}^c)^{\frac{3}{2}}-3X_{pm}^c \tag{11}$$

where $X_p^c=X_{pm}^c+X_{pb}^c$, and $X_{pm}^c=R_1X_{pb}^c$. X_p^c can be expressed as a function of R_1, and a set of conservative expressions are given here by fitting, as follows:

$$X_p^c=\begin{cases}0.499+0.526R_1-0.605R_1^2+0.223R_1^3, 0\le R_1\le 1;\\ 0.695-0.064R_1+0.011R_1^2-9.316\mathrm{e}^{-4}R_1^3+3.056\mathrm{e}^{-5}R_1^4, 1< R_1\le 10;\\ 0.581-0.008R_1+3.425\mathrm{e}^{-4}R_1^2-5.661\mathrm{e}^{-6}R_1^3, 10< R_1\le 20;\\ 0.5, (R_1>20).\end{cases} \tag{12}$$

The proposed fitting expressions in Eq. 12 are all conservative compared to the theoretical solutions. When $0\le R_1\le 20$, the comparisons between the fitting solutions and the theoretical solutions are shown in Fig. 9(a)-(c), and the differences are all within 0.7%. When $0\le R_1\le 1$, X_p^c increases first and then decreases with the increase of R_1. When $1< R_1\le 10$ and $10< R_1\le 20$, X_p^c decreases with the increase of R_1, but the latter segment decreases more slowly. When $R_1>20$, X_p^c decreases monotonically from 0.515(R_1=20) to 0.5($R_1\to\infty$), therefore, X_p^c is conservatively taken as 0.5 in this segment for convenience.

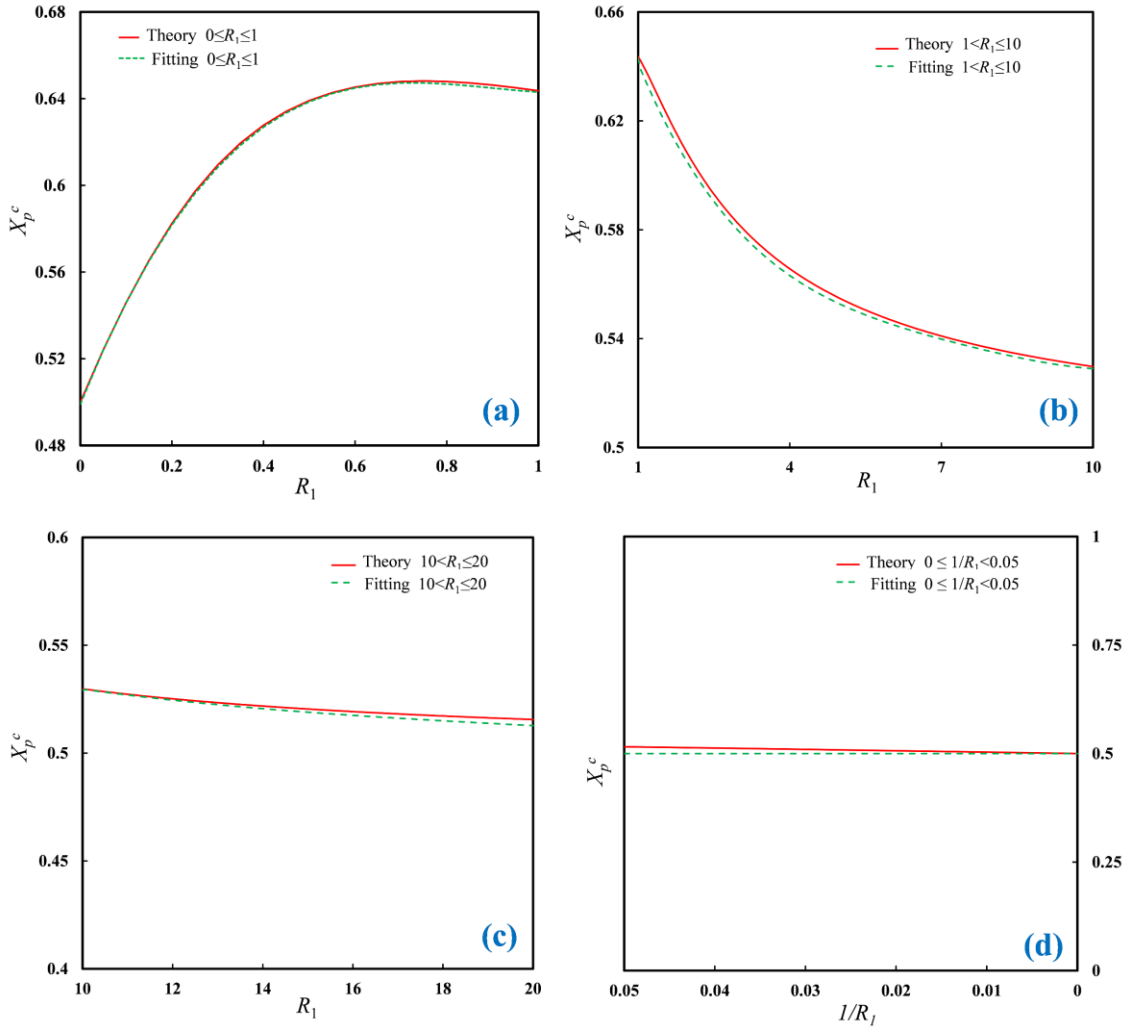

Fig. 9. Comparisons between theoretical and fitting solutions for X_p^c.

Since both X_p^c and X_p^f are only related to R_1, once the parameter R_1 is determined, X_p^c and X_p^f can be obtained through simple calculation, then the corresponding shakedown region can be constructed. Therefore, the parametric equation of the shakedown boundaries can be expressed as:

$$Y'=\begin{cases} 2, 0 \le X_p \le X_p^c \\ \dfrac{2(X_p - X_p^f)}{X_p^c - X_p^f}, X_p^c < X_p \le X_p^f \end{cases} \tag{13}$$

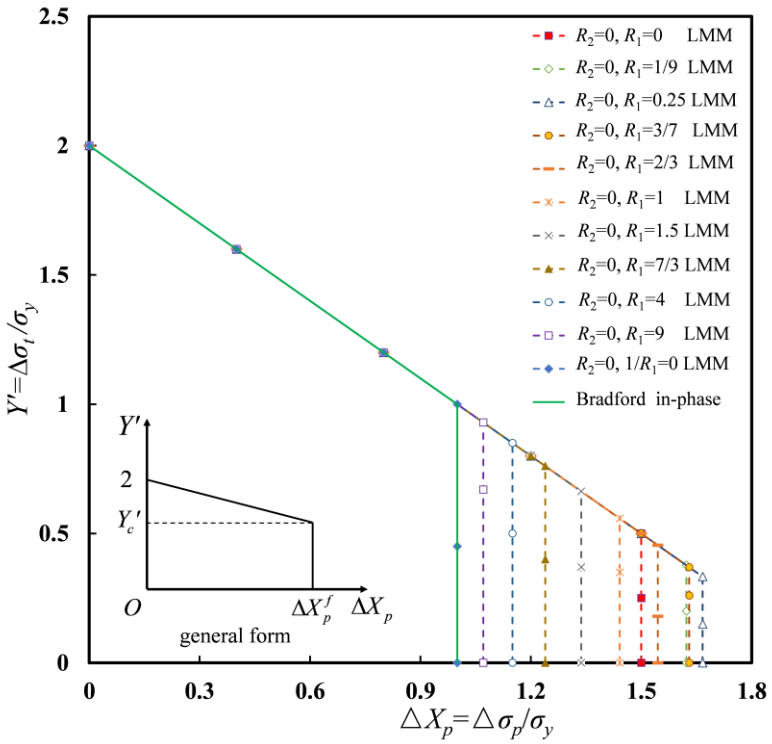

Fig. 10. Shakedown limit calculated results under loading case II when R_2=0, where $\Delta\sigma_p=\Delta\sigma_{pm}+\Delta\sigma_{pb}$ and $Y'=Y$ in this example. The green solid line is the theoretical solution of the shakedown boundary for the Bree problem considering in-phase loading derived by Bradford[31]. The general form of the shakedown boundaries is summarised in the figure according to the numerical results and theoretical solution.

Fig. 10 shows the results for the loading case II, where the abscissa represents the dimensionless primary stress range. The results show that with the gradual increase of R_1, the shakedown regions also increase first and then decrease. When $1/R_1=0$, the area of the shakedown region will reach the minimum, as shown by the green solid line in Fig. 10, which is equivalent to the shakedown boundary of the in-phase loading Bree problem derived by Bradford [31]. For different values of R_1, the shakedown boundaries are all composed of two sections, one of which is controlled by the 3S criterion line ($\Delta X_{pm}+\Delta X_{pb}+Y'=2$), and the other is controlled by the corresponding limit load range ΔX_p^f under the given R_1 value. According to $\Delta X_p^f=X_p^f$, Eq. (14) holds.

$$\Delta X_p^f = \frac{(1+R_1)(\sqrt{9R_1^2+1}-1)}{3R_1^2} \tag{14}$$

Therefore, for loading case II, the parametric equation of the shakedown boundaries can be expressed as:

$$\Delta X_p = \begin{Bmatrix} 2-Y', Y_c' \le Y' \le 2 \\ \Delta X_p^f, 0 \le Y' \le Y_c' \end{Bmatrix} \tag{15}$$

where $Y_c' = 2 - \Delta X_p^f$. The results in Section 4.1 show that the shakedown boundaries are independent of the R_2 value when R_1 is given under in-phase loading. The results in this section prove that the value of R_1 will affect the extent of the shakedown regions when R_2 is given. Therefore, R_1 is the only key control parameter under in-phase loading. However, for loading case I, the results of Fig. 5 and Fig. 8 show that the values of R_1 and R_2 will both affect the extent of the shakedown regions.

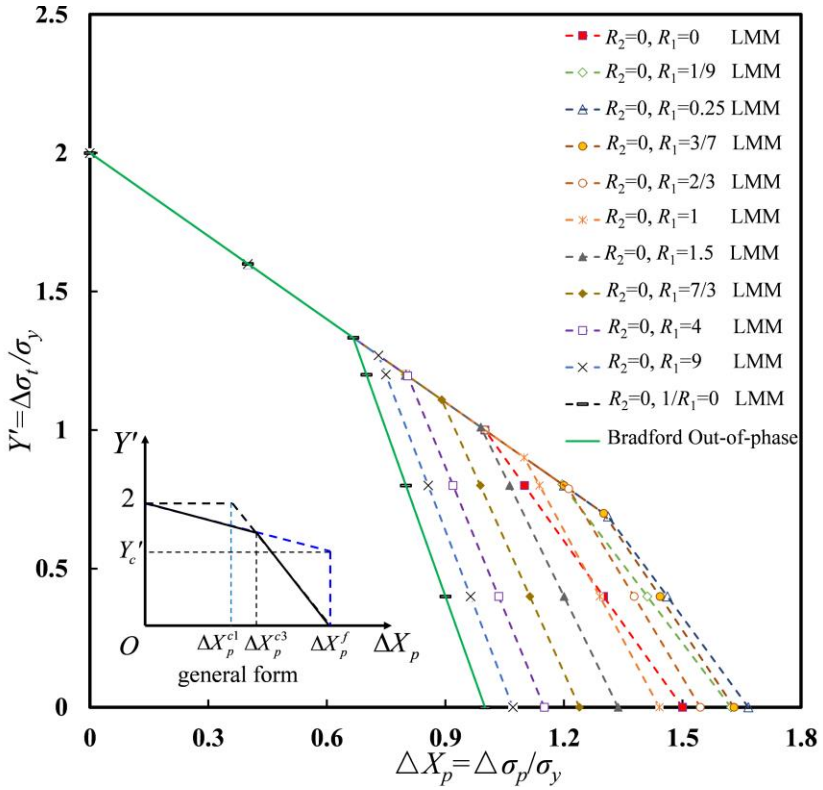

Fig. 11. Shakedown limit calculated results under loading case III when R_2=0, where $\Delta\sigma_p = \Delta\sigma_{pm} + \Delta\sigma_{pb}$ and $Y' = Y$ in this example. The general form of the shakedown boundaries is summarised in the lower-left corner, where the black and blue dotted lines denote the corresponding shakedown boundaries for loading case I and case II. The green solid line is the theoretical solution of the shakedown boundary for the "positive out-of-phase" loading Bree problem derived by Bradford[30].

Fig.11 shows the shakedown limits of loading case III. When $1/R_1 = 0$, the calculation results agree well with the shakedown boundary of the out-of-phase loading Bree problem given by Bradford [30].

According to the relationships among the shakedown boundaries of three loading cases described above, the parametric equation of the shakedown boundaries for loading case III can be deduced, as follows:

$$Y'=\begin{cases} 2-\Delta X_p, 0\le \Delta X_p \le \Delta X_p^{c3} \\ \dfrac{2(\Delta X_p-\Delta X_p^f)}{\Delta X_p^{c1}-\Delta X_p^f}, \Delta X_p^{c3} < \Delta X_p \le \Delta X_p^f \end{cases} \tag{16}$$

where $\Delta X_p^{c1}=X_p^c$， ΔX_p^{c3} can be determined by Eq. (17).

$$\Delta X_p^{c3}=\frac{2\Delta X_p^{c1}}{2+\Delta X_p^{c1}-\Delta X_p^f} \tag{17}$$

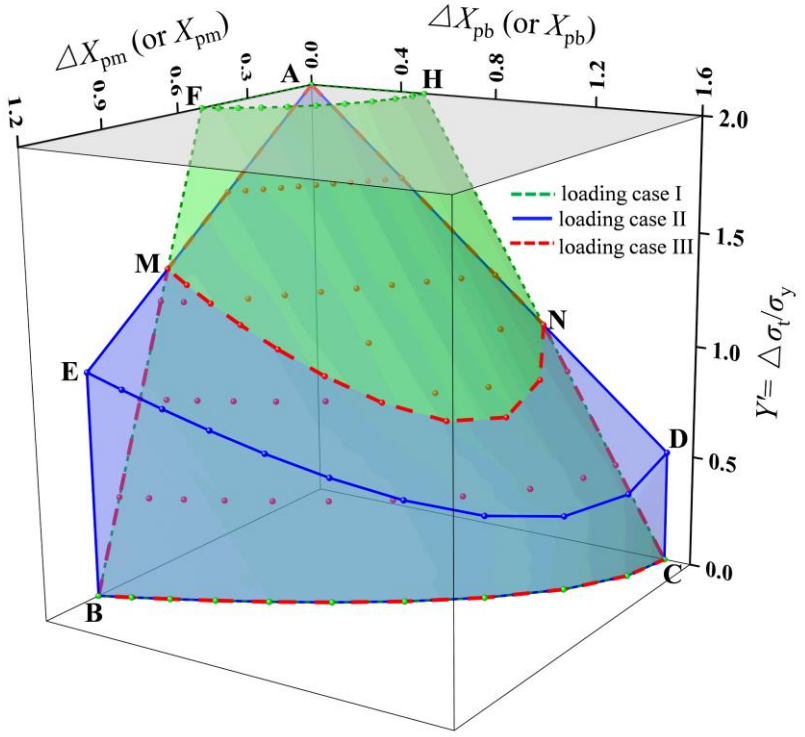

Fig. 12. Three-dimensional shakedown domains under different loading conditions when R_2=0， where the domain AFBCNH indicated by the green dotted lines corresponds to loading case I; the domain AEBCD indicated by the blue solid lines corresponds to loading case II, and the domain AMBCN indicated by the red dotted lines corresponds to loading case III. For loading case I, the coordinate system is $X_{pm}X_{pb}Y'$. For loading case II and loading case III, the coordinate system is $\triangle X_{pm}\triangle X_{pb}Y'$. In this example, $Y'=Y$ represents the dimensionless thermal bending stress.

Fig.12 shows the corresponding three-dimensional elastic shakedown domains for the three types of loading cases. The shakedown domain for loading case I is enclosed by plane AFH and surface FBCH, indicated by the green dashed lines. The shakedown domain for loading case II is enclosed by plane AED and surface EBCD, indicated by the blue solid lines. The shakedown domain for loading case III is enclosed by surfaces AMN and MBCN, indicated by the red dashed lines.

Since formulas (13), (15) and (16) are only simple functions of R_1, the complex 3D shakedown boundaries have been greatly simplified. The newly proposed parametric equations are intuitive, which are more suitable for engineering analysis and design. The analytical solution to loading case I has been extended to generalised loading conditions that enable a broader application scope.

4.3 Pure thermal membrane stress case ($1/R_2$=0)

When $\Delta\sigma_{sb}=0$, the ratcheting boundary expression under loading case I can degenerate from Eq. (2) as follows:

$$\sigma_{\mathrm{pb}}=\frac{3}{4}\left(2\sigma_y-\Delta\sigma_{\mathrm{sm}}\right)+\frac{3\sigma_{\mathrm{pm}}^2}{\Delta\sigma_{\mathrm{sm}}-2\sigma_y} \tag{18}$$

When $\sigma_{\mathrm{pm}}=0$, Eq. (18) can be reduced to the inverse Bree problem; when $\Delta\sigma_{sm}=0$, Eq. (18) can be reduced to Eq. (9).

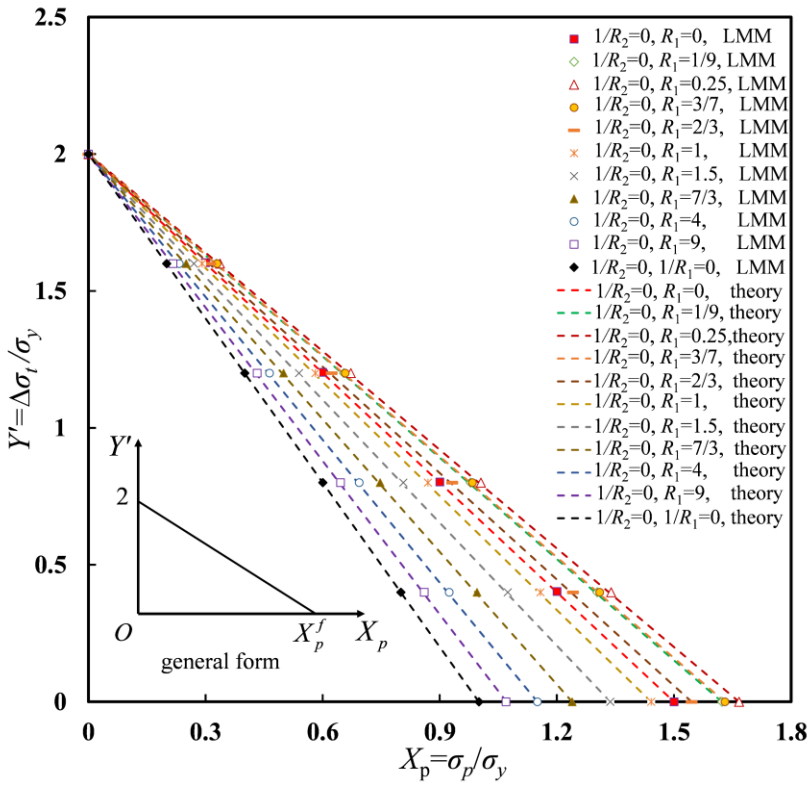

Fig. 13. Comparisons of the shakedown limit calculated results and theoretical solutions (Eq.(18)) under loading case I when $1/R_2$=0. The calculated results are shown by scatter points of various shapes, and theoretical solutions are presented by dotted lines. The abscissa represents the sum of the dimensionless primary membrane and bending (X_{p}= X_{pm}+ X_{pb}), and the ordinate represents the dimensionless pure thermal membrane (Y'=Z) in this case.

For loading case I, the calculation results of shakedown limits are shown in Fig. 13. It is shown that the numerical results agree well with the theoretical solutions (Eq. (18)). With the gradual increase of R_1, the shakedown regions still increase first and then decrease. For any given value of R_1, the corresponding parametric equation of the shakedown boundaries can be expressed as:

$$Y'=2(1-\frac{X_p}{X_p^f}),\quad \text{for } 0\le X_p\le X_p^f \tag{19}$$

When $R_1=0$, the shakedown boundary governing equation is as follows:

$$Y'=2(1-\frac{2}{3}X_{pb}) \tag{20}$$

When $1/R_1=0$, the shakedown boundary governing equation is as follows:

$$Y'=2(1-X_{pm}) \tag{21}$$

Eq. (20) corresponds to the inverse Bree problem, and Eq. (21) corresponds to the checking condition for thermal membrane in the ASME VIII-2 code.

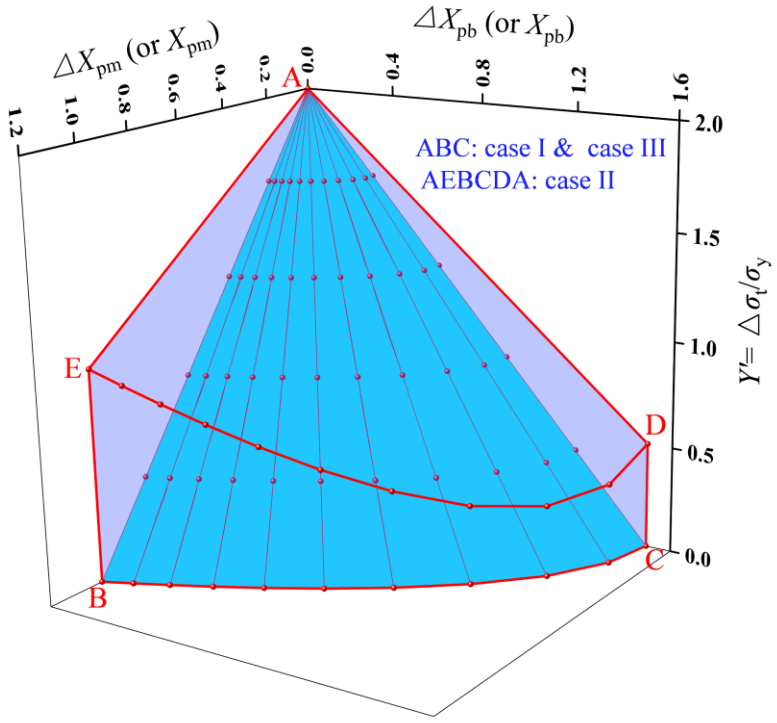

Fig. 14. Three-dimensional shakedown domains under different loading conditions when $1/R_2=0$, where the domain ABC corresponds to loading case I and loading case III; the domain AEBCDA corresponds to loading case II. For loading case I, the coordinate system is $X_{pm}X_{pb}Y'$. For loading case II and loading case III, the coordinate system is $\triangle X_{pm}\triangle X_{pb}Y'$.

For loading case II, the calculation results of shakedown limits are consistent with Fig. 10, so the parametric equation of the shakedown boundaries can be expressed by Eq. (15). Fig. 14 displays the 3D

shakedown domains under different loading conditions, in which the domain ABC corresponds to loading case I, and the domain surrounded by plane AED and surface EBCD corresponds to loading case II. As shown in Fig. 14, the domain ABC also corresponds to loading case III, but the primary stress ranges should be taken as the coordinate axes. Therefore, the parametric equation of the shakedown boundaries under loading case III can be expressed as:

$$Y'=2(1-\frac{\Delta X_p}{\Delta X_p^f}),\quad \text{for } 0\le \Delta X_p \le \Delta X_p^f \tag{22}$$

5. A unified shakedown evaluation scheme for the four-stress parameters Bree-type problems

Shakedown evaluation methods based on the proposed parametric equations can consider the variation of the membrane bending ratios and almost do not lose the accuracy of the original theory. However, the parametric equations need to be constructed separately for each thermal stress distribution situation. Usually, a general and unified evaluation scheme is often needed in engineering, such as the thermal stress ratcheting assessment in the ASME code. Therefore, it is necessary to propose a similar unified shakedown evaluation method for the four-stress parameters Bree-type problem.

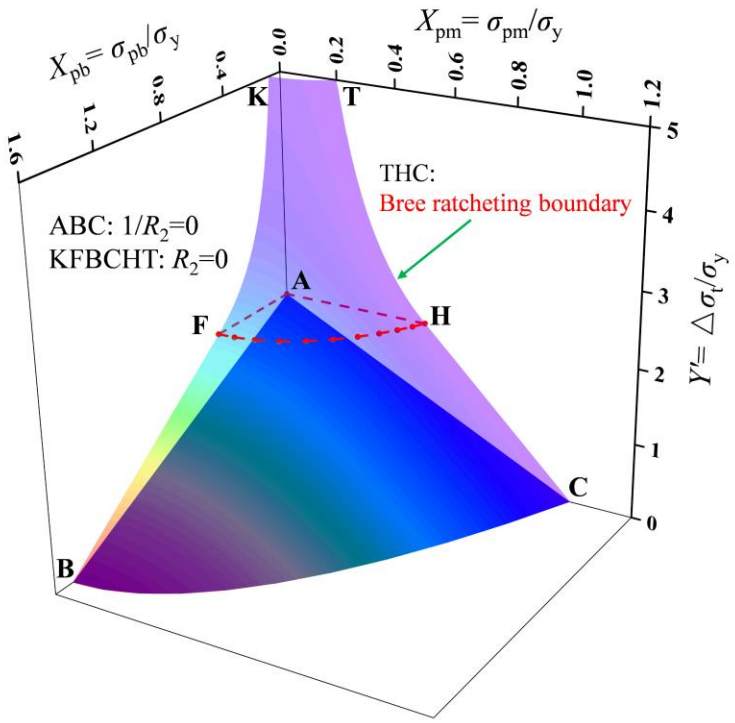

Fig. 15. Ratcheting boundaries of R_2=0 (pure thermal bending, surface KFBCHT) and $1/R_2$=0 (pure thermal membrane, surface ABC) for the four-stress parameters Bree-type problem under loading case I, where curve THC is the Bree ratcheting boundary, and the classical two-dimensional Bree diagram is located in the X_{pb} = 0 plane.

The thermal ratcheting assessment rule given by ASME VIII-2 is actually a conservative representation of the Type-A three-stress parameters Bree-type problem [50,57,80]. Ratcheting boundaries of two typical thermal stress cases (R_2=0 and $1/R_2$=0) are adopted for ratcheting assessment. Similarly, based on the four-dimensional ratcheting boundary theory [56], the ratcheting boundaries for cases of R_2=0 (pure thermal bending) and $1/R_2$=0 (pure thermal membrane) are displayed in Fig. 15. For the case of R_2=0 , the curved surface KBCT is the ratcheting boundary. Section AFH is the alternating plasticity boundary under this situation, which together with the curved surface FBCH encloses the elastic shakedown domain. For the case of $1/R_2$=0 , the curved surface ABC is the ratcheting boundary, and the alternating plasticity boundary degenerates to point A. As shown in Fig. 14, the surface ABC is also the elastic shakedown boundary at this time.

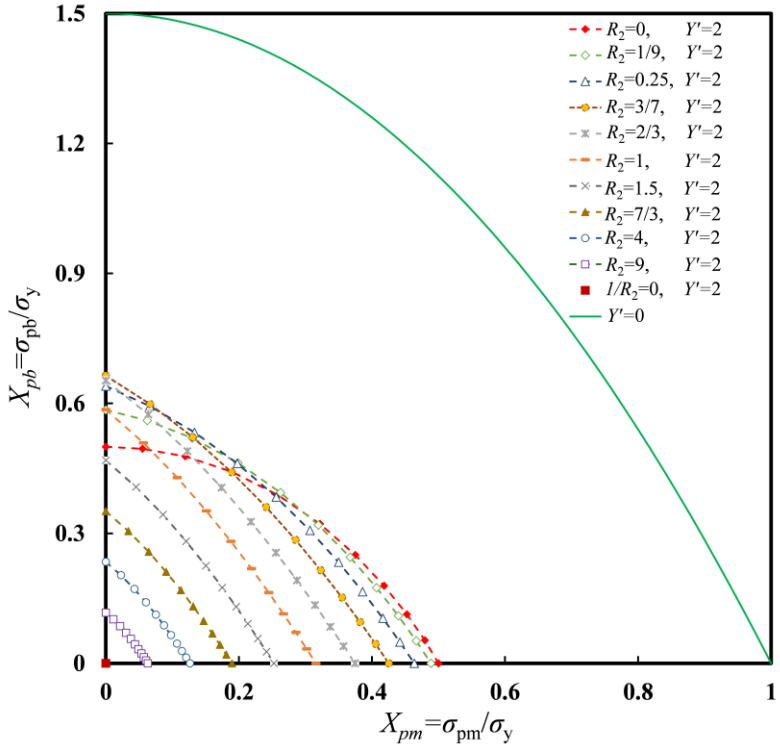

Fig. 16. Projection diagrams of the alternating plasticity boundaries (Y'=2) on the plane Y'=0, where the dotted lines are calculated based on the four-dimensional ratcheting boundary theory, and a series of R_2 values are selected to represent different thermal stress distributions. The red dotted line corresponds to FH in Fig.15, and the green solid line corresponds to BC in Fig.15.

In fact, when $R_2 \geq 0$, the four-dimensional ratcheting boundary can be displayed in the three-dimensional coordinate system of Fig. 15. Curve BC on the plane of Y'=0 is common to all ratcheting boundaries, but the alternating plasticity boundaries on the plane of Y'=2 under different thermal stress distributions are different. Fig. 16 presents the projections of the alternating plasticity boundaries (Y'=2 ,

indicated by dashed lines) under a series of given thermal stress distributions on the $X_{pm}X_{pb}$ plane (Y'=0), in which the red dotted line and green solid line correspond to curve FH and curve BC respectively in Fig. 15. Based on Figs. 15 and 16, it can be concluded that although the ratcheting boundaries change with R_2, there must be a minimum ratcheting boundary. Obviously, the surface ABC is the minimum ratcheting boundary and also the minimum elastic shakedown boundary. This conclusion can also be verified through theoretical analysis. When $Y'>2$, the intersection Y_i' of the ratcheting boundary and the Y' axis can be solved through the four-dimensional ratcheting boundary theory. For $R_2>1$, $Y_i'=2(R_2+1)/(R_2-1)$. Therefore, when $R_2\to+\infty$, Y_i' tends to the minimum value of 2, which corresponds to the case of pure thermal membrane. For $0\le R_2\le 1$, there is no intersection between the ratcheting boundaries and Y' axis; that is, when $X_p\to 0$, Y' tends to infinity, such as the case of pure thermal bending. Based on the idea of a minimum shakedown boundary, we can propose a unified and conservative shakedown assessment scheme for the four-stress parameters Bree-type problems.

For loading case I, Eq. (23) can be adopted for the unified elastic shakedown assessment, as follows:

$$\sigma_{\mathrm{pb}}=\frac{3}{4}\left(2\sigma_y-\Delta\sigma_t\right)+\frac{3\sigma_{\mathrm{pm}}^2}{\Delta\sigma_t-2\sigma_y} \tag{23}$$

Eq. (23) replaces $\Delta\sigma_{\mathrm{sm}}$ in Eq. (18) with $\Delta\sigma_t$, that is, Eq. (23) is applicable to any $R_2\ge 0$ value. In addition, Eq. (23) can also be used as a unified ratcheting assessment method for the four-stress parameters Bree-type problem, but since the plastic shakedown region is ignored, Eq. (23) is very conservative when used in ratcheting assessment.

For loading case II, the shakedown regions are only affected by R_1. It is very convenient to use Eq. (15) proposed in Section 4.2 for shakedown evaluation.

For loading case III, Eq. (24) is proposed for unified elastic shakedown evaluation, as follows:

$$\Delta\sigma_{\mathrm{pb}}=\frac{3}{4}\left(2\sigma_y-\Delta\sigma_t\right)+\frac{3\Delta\sigma_{\mathrm{pm}}^2}{\Delta\sigma_t-2\sigma_y} \tag{24}$$

Eq. (24) replaces σ_{pb} in Eq. (23) with $\Delta\sigma_{\mathrm{pb}}$, and σ_{pm} with $\Delta\sigma_{\mathrm{pm}}$, so it can be applied to generalised thermo-mechanical loading conditions.

It is worth noting that the accuracy of the established parametric equations under the three loading cases has been verified by the LMM, and the elastic shakedown evaluation methods proposed in this section are conservative under the theoretical framework of four-stress parameters Bree-type shakedown and ratcheting problems. In order to be extended to engineering applications, the parametric equations and shakedown evaluation methods proposed in this paper need to be further compared and verified with typical engineering components in the future.

6. Conclusions

In this paper, the four-stress parameters Bree-type shakedown problems (involving two types of membrane and bending stresses) are systematically studied numerically based on the LMM and theoretically based on the four-dimensional ratcheting boundary theory under three typical thermo-mechanical loading conditions to reveal the shakedown mechanisms of four-dimensional Bree diagram.

A detailed discussion on the mechanical models for various uniaxial Bree-type problems has been conducted to clarify the scope of application and mechanical assumptions of each problem. The four kinds of Bree-type problems considered in Section 2 are both relevant and different. The relevance is that they are all derived based on the uniaxial rectangular section beam and can degenerate into the classical Bree problem. The differences lie in the number of stresses considered, the derivation method, the deformation assumptions and the applicable structures. Generally speaking, the two-stress parameters and Type-A three-stress parameters Bree-type problems are applicable to radial ratcheting of axisymmetric thin-walled cylinders. In contrast, the Type-B three-stress parameters and four-stress parameters Bree-type problems are applicable to axial ratcheting of straight pipes.

A common FE model is developed based on the modified two-plane model for all discussed Bree-type problems to facilitate numerical research and comparison. Compared with the Type-A three-stress parameters problem, the four-stress parameters problem does not restrict the bending rotation of the stress section, which makes the latter more conservative. The four-stress parameters problem can degenerate into the Type-B three-stress parameters problem, which can then be degenerated into the two-stress parameters original Bree problem.

Through the newly introduced membrane bending ratio parameters R_1 and R_2, the variation laws of the four-dimensional shakedown boundaries under three loading conditions are revealed based on the LMM. The corresponding semi-analytical parametric equations of the shakedown boundaries under two common thermal stress distributions are constructed based on the numerical results and four-dimensional ratcheting boundary theory. The theoretical solutions with limited application scope can be extended to more general loading conditions. It is found that R_1 and R_2 will both affect the shakedown boundaries under loading case I and loading case III, whereas the shakedown boundaries are only related to R_1 under loading case II.

Based on the idea of a minimum shakedown boundary for the four-stress parameters Bree-type problem, a unified and conservative shakedown evaluation scheme considering generalised loading conditions and variable thermal stress distributions is proposed. The new assessment methods can significantly simplify the shakedown analysis and reduce the cost in the structural design of pressure equipment.

The classical two-stress parameters Bree problem lays the foundation of shakedown design and ratcheting assessment of mainstream codes such as ASME, and is a special case of the four-stress parameters Bree-type problem. Therefore, shakedown mechanisms revealed in this paper are of considerable theoretical

and engineering implications for the structural integrity assessment of industrial components subjected to variable thermal and mechanical loads.

Acknowledgements

This work is supported by the National Natural Science Foundation of China (51828501, 52150710540, 11672147) and the Major Project of National Natural Science Foundation of China (12090033).

Appendix A. Numerical procedure of the LMM for strict shakedown analysis

The upper bound procedure of LMM for strict shakedown analysis is adopted in this paper. Koiter's upper bound shakedown theorem states that: If there exists a kinematically admissible strain rate history and the work done by the body and surface forces on the corresponding plastic strain in the process of repeated loading is greater than the internal plastic dissipation, then the structure will not shake down. According to the Koiter's theorem, the mathematical programming formulation for upper bound can be expressed by Eqs. (A1)-(A4), as follows:

$$\text{min:} \quad \lambda = \frac{\int_0^t dt \int_V D_F(\dot{\varepsilon}_{ij}) dV}{\int_0^t dt \int_V \sigma_{ij}^E \dot{\varepsilon}_{ij} dV} \tag{A1}$$

$$s.t. \quad \Delta\varepsilon_{ij}^n = \int_0^t \dot{\varepsilon}_{ij} dt = \frac{1}{2}(\Delta u_{i,j} + \Delta u_{j,i}) \quad \text{in } V \tag{A2}$$

$$\Delta u_i = \int_0^t \dot{u}_i dt \quad \text{in } V \tag{A3}$$

$$\Delta u_i = 0 \quad \text{on } S_u \tag{A4}$$

In the above formulas, $\dot{\varepsilon}_{ij}$ is the plastic strain rate, $D_F(\dot{\varepsilon}_{ij})$ is the plastic dissipation function, Δu_i is the plastic displacement increment, λ is the load multiplier, σ_{ij}^E is the fictitious elastic stress field caused by external loads, V is the volume of an ideal elastoplastic structure body, S_u is part of the surface and satisfies the zero-displacement rate.

When an elastoplastic structure subjected to varying thermomechanical loads shakes down, the stress history is as follows:

$$\sigma_{ij}(x,t) = \lambda\left[\lambda_p \hat{\sigma}_{ij}^P(x,t) + \lambda_T \hat{\sigma}_{ij}^T(x,t)\right] + \bar{\rho}_{ij}(x) \tag{A5}$$

where $\hat{\sigma}_{ij}^{P}(x,t)$ and $\hat{\sigma}_{ij}^{T}(x,t)$ are elastic stress fields of mechanical and thermal loads, respectively, $\bar{\rho}_{ij}(x)$ denotes a constant residual stress field. The idea of energy minimisation is adopted to solve the shakedown limit multiplier, and the incremental formulation of the energy function is given by:

$$I\left(\Delta\varepsilon_{ij}^{n},\lambda\right)=\sum_{n=1}^{N}\int_{V}\left[\sigma_{ij}^{n}\Delta\varepsilon_{ij}^{n}-\left(\lambda\hat{\sigma}_{ij}\left(t_n\right)+\bar{\rho}_{ij}\right)\Delta\varepsilon_{ij}^{n}\right]dV \tag{A6}$$

where $\Delta\varepsilon_{ij}^{n}$ denotes the plastic strain increment, n denotes the load instance. For load instance n and kth iteration, suppose $\Delta\varepsilon_{ij}^{nk}$ are known, and the shear modulus $\bar{\mu}^{nk}$ of the equivalent linear elastic material can be obtained by Eq. (A7), and $\bar{\varepsilon}$ denotes the von Mises equivalent strain.

$$\frac{3}{2}\bar{\mu}^{nk}\bar{\varepsilon}(\Delta\varepsilon_{ij}^{nk})=\sigma_{y} \tag{A7}$$

When $\bar{\mu}^{nk}$ are known, the following incompressible linear relationship can be proposed:

$$\Delta\varepsilon_{ij}^{n(k+1)\prime}=\frac{1}{2\bar{\mu}^{nk}}\left[\lambda\hat{\sigma}_{ij}'\left(t_n\right)+\bar{\rho}_{ij}^{(k+1)\prime}\right] \tag{A8}$$

Superscript $'$ in Eq. (A8) indicates deviatoric variables. By adding the $\Delta\varepsilon_{ij}^{n(k+1)\prime}$ over a cycle, we can obtain:

$$\Delta\varepsilon_{ij}^{(k+1)\prime}=\sum_{n}\Delta\varepsilon_{ij}^{n(k+1)\prime}=\frac{1}{2\bar{\mu}^{k}}\left[\lambda\sigma_{ij}^{in\prime}+\bar{\rho}_{ij}^{(k+1)\prime}\right] \tag{A9}$$

where $\Delta\varepsilon_{ij}^{(k+1)}$ meets the strain compatible condition. $\frac{1}{\bar{\mu}^{k}}$ and σ_{ij}^{in} can be expressed as:

$$\frac{1}{\bar{\mu}^{k}}=\sum_{n}\frac{1}{\bar{\mu}^{nk}} \tag{A10}$$

$$\sigma_{ij}^{in}=\bar{\mu}^{k}\sum_{n}\frac{\lambda\hat{\sigma}_{ij}\left(t_n\right)}{\bar{\mu}^{nk}} \tag{A11}$$

Through repeated iteration of Eq. (A9), the energy function $I\left(\Delta\varepsilon_{ij}^{n},\lambda\right)$ tends to be minimised gradually to approach the shakedown limit multiplier, which is given by:

$$\lambda^{S}=\frac{\int_{V}\left(\sigma_{y}\sum_{n=1}^{N}\bar{\varepsilon}\left(\Delta\varepsilon_{ij}^{n}\right)\right)dV}{\int_{V}\left(\sum_{n=1}^{N}\hat{\sigma}_{ij}\left(t_n\right)\Delta\varepsilon_{ij}^{n}\right)dV} \tag{A12}$$

References

[1] Peng H, Liu Y, Chen H.F., Shen J. Shakedown analysis of engineering structures under multiple variable mechanical and thermal loads using the stress compensation method. Int. J. Mech. Sci. 2018;140:361-75.
[2] Ma Z, Wang X, Chen H.F., Xuan F-Z, Liu Y. A unified direct method for ratchet and fatigue analysis of structures subjected to arbitrary cyclic thermal-mechanical load histories. Int. J. Mech. Sci. 2021; 194: 106190.

[3] Zheng X, Chen H.F., Ma Z. Shakedown boundaries of multilayered thermal barrier systems considering interface imperfections. Int. J. Mech. Sci. 2018; 144: 33-40.
[4] Peng H, Liu Y, Chen H. A numerical formulation and algorithm for limit and shakedown analysis of large-scale elastoplastic structures. Comput Mech. 2019; 63(1): 1-22.
[5] Cinoglu I S, Begley M R, Deaton J D, Beran P S, McMeeking R M, Vermaak N. Elastoplastic design of beam structures subjected to cyclic thermomechanical loads. Thin Wall Struct. 2019; 136: 175-85.
[6] Zhang Z, Wang S, Brown B, Cinoglu I S, Vermaak N, Lou L H, et al. High temperature shakedown of a 2nd generation nickel-base single crystal superalloy under tension-torsion loadings. Mat Sci Eng A-Struct, 2022; 832: 142457.
[7] Moslemi N, Mozafari F, Abdi B, Gohari S, Redzuan N, Burvill C, et al. Uniaxial and biaxial ratcheting behavior of pressurized AISI 316L pipe under cyclic loading: Experiment and simulation. Int. J. Mech. Sci. 2020; 179: 105693.
[8] Skamniotis C, Courtis M, Cocks A C F. Multiscale analysis of thermomechanical stresses in double wall transpiration cooling systems for gas turbine blades. Int. J. Mech. Sci. 2021; 207: 106657.
[9] Hasbroucq S, Oueslati A, de Saxcé G. Analytical study of the asymptotic behavior of a thin plate with temperature-dependent elastic modulus under cyclic thermomechanical loadings. Int. J. Mech. Sci. 2012; 54(1): 95-104.
[10] Liu F, Gong J-G, Chen H.F., Xuan F-Z. A direct approach to progressive buckling design considering ratcheting deformation. Thin Wall Struct. 2021; 163: 107656.
[11] Foroutan M, Ahmadzadeh G R, Varvani-Farahani A. Axial and hoop ratcheting assessment in pressurized steel elbow pipes subjected to bending cycles. Thin Wall Struct. 2018; 123: 317-23.
[12] Leu S Y, Li J S. Shakedown analysis of truss structures with nonlinear kinematic hardening. Int. J. Mech. Sci. 2015; 103: 172-80.
[13] Zeinoddini M, Mo'tamedi M, Gharebaghi S A, Parke G A R. On the ratcheting response of circular steel pipes subject to cyclic inelastic bending: A closed-form analytical solution. Int. J. Mech. Sci. 2016, 117: 243-57.
[14] Pham D C. Consistent limited kinematic hardening plasticity theory and path-independent shakedown theorems. Int. J. Mech. Sci. 2017; 130: 11-8.
[15] Abdalla H F. Effect of wall thinning on the shakedown interaction diagrams of 90-degree back-to-Back bends subjected to simultaneous steady internal pressures and cyclic in plane bending moments. Thin Wall Struct. 2019; 144: 106228.
[16] Shariati M, Kolasangiani K, Golmakani H. Cyclic behavior of SS316L cylindrical shells under pure torsional load: An experimental investigation. Thin Wall Struct. 2016; 109: 242-50.
[17] Zeinoddini M, Mo'tamedi M, Zandi A P, Talebi M, Shariati M, Ezzati M. On the ratcheting of defective low-alloy, high-strength steel pipes (API-5L X80) under cyclic bending: An experimental study. Int. J. Mech. Sci. 2017; 130: 518-33.
[18] Chen X, Chen H, Zhao L. Ratcheting behavior of pressurized corroded straight pipe subjected to cyclic bending. Thin Wall Struct. 2019; 145: 106410.
[19] Zhang J, Oueslati A, Shen W Q, De Saxcé G, Nguyen A D, Zhu Q Z, et al. Shakedown analysis of a hollow sphere by interior-point method with non-linear optimization. Int. J. Mech. Sci. 2020; 175: 105515.
[20] Liu C, Yu D, Akram W, Cai Y, Chen X. Ratcheting behavior of pressurized elbow pipe at intrados under different loading paths. Thin Wall Struct. 2019; 138: 293-301.
[21] Zhang J, Shao J F, Zhu Q Z, De Saxcé G. A variational-based homogenization model for plastic shakedown analysis of porous materials with a large range of porosity. Int. J. Mech. Sci. 2021; 199: 106429.
[22] Mo'tamedi M, Zeinoddini M, Elchalakani M. A closed-form analytical solution for the ratcheting response of steel tubes with wall-thinning under inelastic symmetric constant amplitude cyclic bending. Thin Wall Struct. 2018; 132: 558-73.
[23] da Costa Mattos H S, Peres J M A, Melo M A C. Ratcheting behaviour of elasto-plastic thin-walled pipes under internal pressure and subjected to cyclic axial loading. Thin Wall Struct. 2015; 93: 102-11.
[24] ASME Boiler & Pressure Vessel Code, VIII Division 2 Alternative Rules, Rules for Construction of Pressure Vessels, 2019.
[25] ASME Boiler & Pressure Vessel Code, III Division 1 NB Class 1 Components, Rules for Construction of Nuclear Facility Components, 2015.
[26] ASME Boiler & Pressure Vessel Code, III Division 1 NH Class 1 Components in Elevared Temperature Service, Rules for Construction of Nuclear Facility Components, 2013.
[27] EN 13445-3. European Standard for Unfired Pressure Vessels—Part 3: Design. 2002.

[28] Bree J. Elastic-plastic behavior of thin tubes subjected to internal pressure and intermittent high-heat fluxes with application to fast-nuclear-reactor fuel elements. J Strain Anal. 1967; 2: 226–38.
[29] Bree J. Incremental growth due to creep and plastic yielding of thin tubes subjected to internal pressure and cyclic thermal stresses. J Strain Anal. 1968; 3(2): 122-27.
[30] Bradford R.A.W. The Bree problem with the primary load cycling out-of-phase with the secondary load. Int. J. Pres. Ves. Pip. 2017; 154:83-94.
[31] Bradford R.A.W. The Bree problem with primary load cycling in-phase with the secondary load. Int. J. Pres. Ves. Pip. 2012; 99: 44-50.
[32] Ng H W, Moreton D N. Alternating plasticity at the surfaces of a Bree cylinder subjected to in-phase and out-of-phase loading. J Strain Anal Eng. 1987; 22(2): 107-13.
[33] Ng H W, Moreton D N. Ratchetting rates for a Bree cylinder subjected to in-phase and out-of-phase loading. J Strain Anal Eng. 1986; 21(1): 1-7.
[34] Osage D A, Dong P, Spring D W. Fatigue assessment of welded joints in API 579-1/ASME FFS-1 2016-existing methods and new developments. Procedia engineering. 2018; 213: 497-538.
[35] Spring D W, Panzarella C, Osage D A. Revisiting the bree diagram. ASME Pressure Vessels & Piping Conference, 2016.
[36] Pei X, Dong P. A universal approach to ratcheting problems of bree type incorporating arbitrary loading and material nonlinearity conditions. Int. J. Pres. Ves. Pip. 2020; 185: 104137.
[37] O'Donnell W J, Porowski J. Upper bounds for accumulated strains due to creep ratcheting. J Pressure Vessel Technol. 1974; 96:150-4.
[38] O'Donnell W J, Porowski J, Badlani M. Simplified inelastic analysis methods for bounding fatigue and creep rupture damage. J Pressure Vessel Technol. 1980;102: 394-9.
[39] Bradford R.A.W, Ure J, Chen H.F. The Bree problem with different yield stresses on-load and off-load and application to creep ratcheting. Int. J. Pres. Ves. Pip. 2014; 113: 32-9.
[40] McGreevy T E, Leckie F A, Carter P, Marriott D L. The effect of temperature dependent yield strength on upper bounds for creep ratcheting. ASME Pressure Vessels & Piping Conference, 2006.
[41] Peng H, Liu Y, Chen H.F. Shakedown analysis of elastic-plastic structures considering the effect of temperature on yield strength: theory, method and applications. Eur. J. Mech. Solid. 2019; 73: 318-30.
[42] Nayebi A. Influence of continuum damage mechanics on the Bree's diagram of a closed end tube. Mat & Des. 2010; 31(1): 296-305.
[43] Surmiri A, Nayebi A, Rokhgireh H. Shakedown-ratcheting analysis of Bree's problem by anisotropic continuum damage mechanics coupled with nonlinear kinematic hardening model. Int. J. Mech. Sci. 2018; 137: 295-303.
[44] Pei X, Dong P, Mei J. The effects of kinematic hardening on thermal ratcheting and Bree diagram boundaries. Thin-Walled Struc. 2021; 159:107235.
[45] Bree J. Plastic deformation of a closed tube due to interaction of pressure stresses and cyclic thermal stresses. Int J Mech Sci. 1989; 31: 865-92.
[46] Nadarajah C, Ng H W. Biaxial Ratcheting and Cyclic Plasticity for Bree-Type Loading—Part II: Comparison Between Finite Element Analysis and Theory. J Pressure Vessel Technol. 1996; 118: 161-7.
[47] Ng H W, Nadarajah C. Biaxial Ratcheting and Cyclic Plasticity for Bree-Type Loading—Part I: Finite Element Analysis. J Pressure Vessel Technol. 1996; 118(2):154-160.
[48] Bradford R A W. Solution of the ratchet-shakedown Bree problem with an extra orthogonal primary load. Int. J. Pres. Ves. Pip. 2015; 129: 32-42.
[49] O'Donnell W J, Porowoski J S. Biaxial model for bounding creep ratcheting. ORNL Report ORNL/Sub7322/2, ORNL, Oak Ridge, TN, 1981.
[50] Reinhardt W. On the interaction of thermal membrane and thermal bending stress in shakedown analysis. ASME Pressure Vessels & Piping Conference, 2008.
[51] Asadkarami A, Reinhardt W. Shakedown at thermal discontinuities involving thermal membrane and thermal bending stress. ASME Pressure Vessels & Piping Conference, 2012.
[52] Adibi-Asl R, Reinhardt W. Non-cyclic shakedown/ratcheting boundary determination–Part 1: Analytical approach. Int. J. Pres. Ves. Pip. 2011; 88: 311-20.
[53] Adibi-Asl R, Reinhardt W. Non-cyclic shakedown/ratcheting boundary determination-Part 2: Numerical implementation. Int. J. Pres. Ves. Pip. 2011; 88: 321-9.
[54] Reinhardt W. A noncyclic method for plastic shakedown analysis. J Press Vess-T ASME. 2008; 130(3): 031209.

[55] ASME Boiler & Pressure Vessel Code, VIII Division 2 Alternative Rules, Rules for Construction of Pressure Vessels, 2013.
[56] Shen J, Chen H.F, Liu Y. A new four-dimensional ratcheting boundary: Derivation and numerical validation. Eur. J. Mech. Solid. 2018; 71: 101-12.
[57] Bao H, Shen J, Liu Y, Chen H.F. Shakedown analysis of modified Bree problems involving thermal membrane stress and generalized loading conditions. Int. J. Pres. Ves. Pip. 2021; 192:104432.
[58] Koiter W T. General theorems for elastic-plastic solids. In: Sneddon JN, Hill R, editors. Progress in solid mechanics. Amsterdam: North-Holland; 1960. p. 167–221.
[59] Melan E. Theorie statisch unbestimmter systeme aus ideal-plastichem baustoff. Sitzungsber d Akad d Wiss 1936;145(2A):195-218.
[60] Makrodimopoulos A , Martin CM . Lower bound limit analysis of cohesive-frictional materials using second-order cone programming. Int J Numer Methods Eng. 2006;66:604–34.
[61] Simon JW , Weichert D . Numerical lower bound shakedown analysis of engineering structures. Comput Methods Appl Mech Eng. 2011;200:2828–39 .
[62] Chen H.F, Ponter A R, Ainsworth R. The linear matching method applied to the high temperature life integrity of structures. Part 1. Assessments involving constant residual stress fields. Int. J. Pres. Ves. Pip. 2006; 83(2):123-135.
[63] Chen H.F, Ponter A R, Ainsworth R. The linear matching method applied to the high temperature life integrity of structures. Part 2. Assessments beyond shakedown involving changing residual stress fields. Int. J. Pres. Ves. Pip. 2006; 83(2): 136-147.
[64] Chen H.F, Ponter A R S. Linear matching method on the evaluation of plastic and creep behaviours for bodies subjected to cyclic thermal and mechanical loading. Int J Numer Meth Eng. 2006; 68(1): 13-32.
[65] Chen H.F, Engelhardt M J, Ponter A R S. Linear matching method for creep rupture assessment. Int. J. Pres. Ves. Pip. 2003; 80(4): 213-20.
[66] Barbera D, Chen H. Creep rupture assessment by a robust creep data interpolation using the Linear Matching Method. Eur J Mech A-Solid, 2015; 54: 267-79.
[67] Barbera D, Chen H.F, Liu Y, Xuan F Z. Recent developments of the linear matching method framework for structural integrity assessment. J Press Vess-T ASME. 2017;139(5): 051101.
[68] Barbera D, Chen H, Liu Y. On creep fatigue interaction of components at elevated temperature. J Press Vess-T ASME. 2016; 138(4): 041403.
[69] Pisano A A, Fuschi P. Mechanically fastened joints in composite laminates: Evaluation of load bearing capacity. Compos Part B-Eng. 2011; 42(4): 949-61.
[70] Pisano A A, Fuschi P, De Domenico D. Peak load prediction of multi-pin joints FRP laminates by limit analysis. Compos Struct. 2013; 96: 763-72.
[71] Pisano A A, Fuschi P. A numerical approach for limit analysis of orthotropic composite laminates. Int J Numer Meth Eng. 2007; 70(1): 71-93.
[72] R5, Assessment Procedure for the High Temperature Response of Structures. Issue 3 Revision 002，EDF Energy Nuclear Generation Ltd., 2014.
[73] Adibi-Asl R, Reinhardt W. Ratchet Limit Solution of a Beam With Arbitrary Cross Section. J Press Vess-T ASME. 2015; 137(3): 031004.
[74] Bhagwagar T, Gurdal R. Straight Pipe Cyclic Analyses for Shakedown Verification Code Criteria. ASME Pressure Vessels & Piping Conference, 2003.
[75] Reinhardt W. Elastic-Plastic Shakedown Assessment of Piping Using a Non-Cyclic Method. ASME Pressure Vessels & Piping Conference, 2007.
[76] Reinhardt W. Distinguishing ratcheting and shakedown conditions in pressure vessels. ASME Pressure Vessels & Piping Conference, 2003; 16990: 13-26.
[77] Jappy A, Mackenzie D, Chen H. A fully implicit, lower bound, multi-axial solution strategy for direct ratchet boundary evaluation: implementation and comparison. J Pressure Vessel Technol. 2014; 136(1): 011205.
[78] Messner M C, Sham T L. Detection of ratcheting in finite element calculations. ASME Pressure Vessels & Piping Conference, 2018-84102, V01BT01A013; 9 pages.
[79] Messner M C, Sham T L, Wang Y. N-bar problems as approximations to the bree problem. ASME Pressure Vessels & Piping Conference, 2018-84106, V01BT01A017; 10 pages.
[80] Shen J, Lu M-W, Bao H, Liu Y. A modification on 3S criterion and simplified elastic-plastic ratcheting analysis in ASME VIII-2. Int. J. Pres. Ves. Pip. 2020;188:104215.